STUDY OF RANDOM FIBRE LASERS AND APPLICATIONS

Dao Xiang

Thesis submitted to the Faculty of Graduate and Postdoctoral Studies
In partial fulfillment of the requirements
for the Degree of
Master of Science in Physics

Ottawa-Carleton Institute for Physics
Department of Physics
University of Ottawa

For my family

Abstract

The properties of two novel random fibre lasers, in which stimulated Brillouin scattering supplies the effective gain mechanism and Rayleigh scattering along the standard telecommunication optical fibre provides random distributed feedback, are characterised. Firstly, ultra-narrow microwave signals with a Dirac delta function profile are successfully created by beating two random-lasing near-Gaussian beams, arising from the synchronization of optical modes from two Stokes signals with random phase accumulated over the ultra-long optical fibre. This finding provides a completely new approach to synthesise high spectral purity microwave signals from Brillouin fibre lasers with randomised feedback. In addition, we also develop a theoretical model of the random fibre Fabry-Pérot resonator based on the fact that the pump depletion effect naturally selects out the effective Rayleigh feedback regions localised in both ends of this long fibre. A narrow random-laser output with the linewidth of ~860 Hz is experimentally demonstrated and is employed to characterise the linewidth of the pump light. Furthermore, the random laser dynamics is studied and one application towards the physical entropy source is eventually achieved.

Acknowledgments

I feel incredibly lucky to have grown up in the Fibre Optics Group where I have benefited from inspired leadership, a diversity of good advice and the freedom to try my ideas and explore.

First and foremost, I would especially like to thank my supervisor Dr. Xiaoyi Bao for her guidance and support throughout my M.Sc study over the past two years. I have benefited tremendously from her rich experience, depth of knowledge and generosity. She is always available to inspire me, give suggestions and share ideas with me. Her passion in scientific research and the way that she interacts with the scientific community will continue to guide me in the future. I also would express my grate gratitude to Dr. Liang Chen for his instructive and insightful suggestions during my research process. I find enormous benefits from his broad perspective and rigorous thinking.

I would especially like to appreciate Dr. Ping Lu who taught me lots of things, frequently discussed with me and answered emails even after midnight during this work. Ping's enthusiasm for experimental work coupled with his wide ranging knowledge and willingness to help has been invaluable throughout this thesis. It is a memorable experience to work together with him on several exciting research projects.

I would also like to give special mention to other people in fibre optics group. In the beginning of my master study, I benefited greatly from the guidance and advice of Dr. Wenhai Li as well as a number of discussions with Yang Lu. I collaborated with Yanping Xu and Zhonghua Ou for the bi-directional pumping random fibre laser project and we shared ideas with each other. I completed courses and attended annual SERA workshop with Yanping and Meiqi Ren, and we experienced many happy moments. Chams Baker, Qian He, Song Gao, Bhavaye Saxena, Yang Li, and Daisy Williams also provided valuable suggestions and encouragement.

I had the opportunity to take courses offered by Robert Boyd and Paul Corkum.

They are inspired and patient teachers, and bring a rare combination of deep theoretical knowledge coupled with a practical understanding of experimental realities to their teaching, which laid the foundations of my graduate work.

Finally, I would like to give my deepest gratitude to my parents for their unwavering support, understanding, and encouragement for all of these years! At last I would like to adequately thank my fiancé Helen for standing by me throughout this endeavour. I am looking forward to our next great adventure together. I dedicate this thesis to them.

Statement of Originality

This work contains no material which has been accepted for the award of any other degree or diploma in any university or other tertiary institution and, to the best of my knowledge and belief, contains no material previously published or written by another person, except where due reference has been made in the text.

I give consent to this copy of my thesis, when deposited in the University Library, being available for loan and photocopying.

SIGNED: _____

DATE: _____

Supervisor: Dr. Xiaoyi Bao

Contents

CV

Publications:

1. **D. Xiang**, P. Lu, Y. Xu, L. Chen, X. Bao, “Physical Random Bit Generation with Random Brillouin Fibre Laser,” unpublished results, 2015.

2. **D. Xiang**, P. Lu, Y. Xu, L. Chen, X. Bao, “Generation of ultra-narrow linewidth microwave signals based on random Brillouin fibre laser,” *Light: Science & Applications*, submitted, 2015.

3. Y. Xu[1], **D. Xiang**[1], Z. Ou, P. Lu, X. Bao, “Random Fabry-Pérot resonator based sub-kHz Brillouin fibre laser to improve spectral resolution in linewidth measurement,” *Opt. Lett.*, vol.40, no.9, pp.1920-1923, 2015. ([1]These Authors contributed equally)

Chapter 1

Introduction

1.1 Motivation

We experience poor visibility in foggy weather. All of what we can see in daily life begins with our eyes that collect light reflected from the surrounding environment or objects. So such opaque white appearance in a foggy day must arise from some physical phenomenon which prevents light rays from reaching our eyes. This phenomenon essentially relevant to our daily lives is multiple scattering. Fog is a suspension of cloud water droplets or ice crystals with a strong tendency to scatter light waves. The light rays from an object are scattered thousands of times by thousands of water droplets, thus leading to blurring the vision. Similar phenomena are also exhibited in other disordered materials like milk, white marble walls [1], and white paint [2].

In the field of photonics, multiple scattering in optical materials in which atoms are imperfectly located in a random pattern paves the way to disordered photonics [1]. One essential and interesting application is random lasing - the new type of disorder-based laser light source. Lasing phenomenon is a story about the carefully controlled balance between gain and loss. The gain is determined by how long photons stay inside the gain medium and the loss relies on how easily photons escape. When the total gain in the cavity is larger than the losses, the laser system reaches a threshold

and lases at resonant frequencies. Let us consider a disordered amplifying medium that is being illuminated by a light beam. The behavior of light rays penetrating disordered optical materials and then multiply scattered by inhomogeneity of the wavelength-scale follows a random walk, resembling the Brownian motion of particles suspended in liquids. Multiple scattering enhances the optical path length inside the gain medium to supply a level of feedback sufficient for approaching the random-lasing threshold. Because optical waves bounce randomly from a particle to another, the term “random laser” was coined [3]. If scattered photons cannot return to their initial locations, the constructive interference will not appear to determine resonant spectral components. So the feedback in such a laser is merely used to return part of the energy to the gain medium and the emission has a continuous optical spectrum with the narrowing gain shape. This kind of lasing system is dubbed as “incoherent feedback” random laser. On the other hand, if some randomly scattered photons undergoing the amplified random walk return to their original positions, interference effects will appear in emission features such as discrete peaks. This is the “coherent feedback” random laser. The transition from the incoherent feedback random lasing to the coherent feedback random lasing can be realised through enhancing the scattering strength, for example, increasing the ZnO particle density in Rhodamine 640 dye solutions [4].

In recent years, the random distributed feedback fibre laser, the new member of the family of random lasers, has become a particularly attractive research direction thanks to its inherent cylindrical waveguide structure to provide an excellent random-

lasing directionality [5]. The intrinsic disorder of a standard telecommunication fibre works as numerous tiny scattering centers. The gain mechanism is created via the distributed Raman effect or the distributed Brillouin effect. Although many literature reviews have claimed that random fibre lasers could hold a variety of potential applications, the uncontrollable nature of random lasing like unstable emission spectra has limited the practical application. My graduate research is to explore the characteristics of two novel random fibre lasers and demonstrate different applications.

1.2 Thesis Contribution

In this thesis, we are dealing with the fibre laser with randomised feedback involving fibre optics, statistical optics, nonlinear optics and microwave photonics.

Firstly, we propose a novel fibre ring laser scheme that the interplay between stimulated Brillouin scattering supplying the effective gain mechanism and random distributed feedback provided by Rayleigh scattering along an ultra-long standard telecommunication optical fibre improves the random lasing directionality and efficiency, leading to unique properties of the random fibre laser. We demonstrated the generation of ultra-narrow microwave signals since a high degree of mutual coherence between two initially incoherent Stokes signals becomes feasible, obtained by beating two random laser beams. The Dirac delta function profile in power spectral density of microwave signals arises from the synchronization of optical modes from two Stokes signals with random phase accumulated over the ultra-long optical fibre. In addition, our approach lightens the burden on the extraordinary demands of pump

sources with narrow linewidth and expensive external optical modulators in conventional systems. Conventional microwave photonic systems require narrow-linewidth optical pumping source to generate two ultra-narrow waves and heterodyne them, or use external optical modulator as the frequency shifter to achieve the self-heterodyne without delay line, leading to the generation of microwave signal in the electrical domain. Moreover, our system has potential for reaching terahertz (THz) frequencies by adopting two independent lasers as pump sources.

We also develop one random Brillouin fibre laser scheme based on random Fabry-Pérot (FP) resonator. The Brillouin gain is built up within the bi-directionally pumped 10-km optical fibre and the distributed Rayleigh scattering partially traps the SBS Stokes photons. A prototype of the random fibre FP resonator is developed based on the fact that the pump depletion effect naturally selects out the effective Rayleigh feedback regions localised in both ends of this long fibre, leading to a narrow lasing with the linewidth of ~860 Hz. In addition, the spectral information of the beat signal by heterodyning such narrow random-lasing emission and the pump light can be used to characterise the linewidth of the pump light. The temporal property is also discussed with an application towards the random bits generator.

Chapter 2

Theoretical Background

Multiple scattering in multi-dimensional structures brings random lasers special features such as an unstable angular beam propagation, low lasing efficiency and non-localised emission spectra. In 2002, Cao and co-workers proposed an analytical model to show the lasing threshold decreases exponentially with the size of the sample in that photons created inside medium require an extremely long time to escape as one-dimensional random lasers operate in the strong localization regime, leading to a decreased demand for the pump power [6]. Optical fibres are excellent candidates thanks to their inherent cylindrical waveguide geometry to transversely confine photons, leading to improved lasing directionality and efficiency. The first work was reported in [7] where the photonic crystal fibre with the hollow core was filled with a suspension of TiO_2 nanoparticles in a Rhodamine 6G dye solution to carry out the incoherent feedback based random lasing. Further, Hu *et al.* experimental developed a coherent random fibre laser by filling a hollow-core optical fibre with a dispersive solution of polyhedral oligomeric silsesquioxanes nanoparticles and laser dye pyrromethene 597 in carbon disulfide [8]. Moreover, both the reduced threshold and increased directionality were demonstrated in this system.

Another random fibre laser schemes are based on the amplification processes and random scattering mechanisms in standard optical fibres, which is the main research

topics of this thesis. Before we discuss such schemes, we should fully characterise different mechanisms in optical fibres. In this chapter, different gain and random feedback mechanisms in optical fibres are firstly introduced. Some classical random fibre laser structures are also discussed. Finally, we give a detailed description of the lasing properties of random Brillouin fibre lasers.

2.1 Gain Mechanisms in Optical Fibres

2.1.1 Gain provided by Stimulated Brillouin Scattering

Brillouin scattering is a dominant optical effect in standard telecommunication fibres. The spontaneous process is initiated by thermally induced fluctuations in the optical properties of optical fibres. An incident photon is scattered from the thermally generated acoustic phonon and transformed into the Stokes photon with frequency downshift and a newly-born phonon. Although the waveguide geometry intrinsically selects only two favored direction including forward and backward, the forward one is very weak due to the wavevector mismatch. If the power of incident light reach the critical value, stimulated Brillouin scattering (SBS) will occur. The backscattered Stokes wave interferes with the incident wave and creates the acoustic wave by the process of electrostriction. The acoustic wave works as a moving grating that continues to scatter the incident wave, which reinforces the optical intensity of the Stokes wave. Therefore, this positive feedback mechanism results in an exponential growth of the amplitude of the Stokes wave.

Equations describing the nonlinear coupling among pump wave, Stokes wave and

density disturbance in the SBS process are shown in Eq. (2.1) [9]:

$$\frac{\partial E_P}{\partial z}+\frac{n}{c}\frac{\partial E_P}{\partial t}=\frac{i\gamma_e\omega_s}{4\rho_0 nc}\rho E_S-\alpha E_P \tag{2.1a}$$

$$\frac{\partial E_S}{\partial z}-\frac{n}{c}\frac{\partial E_S}{\partial t}=\frac{i\gamma_e\omega_P}{4\rho_0 nc}\rho^* E_S+\alpha E_S \tag{2.1b}$$

$$\upsilon\frac{\partial \rho}{\partial z}+\frac{\partial \rho}{\partial t}+\frac{1}{2}\Gamma_B\rho=\frac{i\gamma_e\varepsilon_0 q^2}{4\Omega}E_S E_L^*+f \tag{2.1c}$$

where E_P, E_S, ω_p and ω_s are the pump wave and the Stokes wave amplitudes and frequencies, respectively; ρ is the complex amplitude of the density variation; n is the mean refractive index of the core and α is the linear loss coefficient; υ, Γ_B and Ω are the sound velocity, the phonon decay rate and the frequency of the acoustic wave respectively; f represents the Langevin noise source describing the thermal excited acoustic wave that initiates the SBS process; γ_e is the electrostrictive constant of fibres expressed by

$$\gamma_e=\rho\frac{\partial \varepsilon}{\rho} \tag{2.2}$$

where ε is the dielectric constant of optical fibres. In the constant-pump limit and the assumption of no loss, Eq. (2.1) can have analytical solutions [10]:

$$E_S(0,t)=\frac{i\gamma_e\omega_S}{4\rho_0 nc}E_P\int_0^t dt'\int_L^0 dz' e^{-\Gamma_B(t-t')/2}f^*(z',t')I_0\{[\frac{\Gamma_B G(z')(t-t')}{L}]^{1/2}\} \tag{2.3}$$

where I_0 is the zeroth order modified Bessel function, and G and I are defined by

$$G=g_B I_P(z=0)L_{eff} \text{ and } I_P=\frac{1}{2}n\varepsilon_0 c|E_P|^2 \tag{2.4}$$

with

$$g_B=\frac{\gamma_e^2\omega_P^2}{n\upsilon c^3\rho_0\Gamma_B} \text{ and } L_{eff}=\frac{1}{\alpha}[1-e^{-\alpha L}] \tag{2.5}$$

In addition, the spectral density function $S(\omega)$ of the Stokes wave can be acquired by the Fourier transform of the autocorrelation function of E_S:

$$S(\omega) = \frac{4h\omega_S(N+1)}{ncA\Gamma_B}[\exp(\frac{G(\frac{\Gamma_B}{2})^2}{\omega^2 + (\frac{\Gamma_B}{2})^2}) - 1] \quad (2.6)$$

where *h*, *N* and *A* are the Plank constant, the mean number of phonons per mode of the acoustic field and the effective cross-section area, respectively. So the spectral shape of Stokes wave depends on not only the phonon decay rate Γ_B but also the single-pass gain *G* in the optical fibre. In the low-gain limit ($G \ll 1$), the spectral shape of spontaneous Brillouin scattering Stokes wave follows Lorentzian profile with a full width at half maximum (FWHM) of $\Delta\omega = \Gamma_B$, while in the high gain limit ($G \gg 1$), the spectral shape of SBS Stokes wave is Gaussian profile with a FWHM expressed by

$$\Delta\omega = \Gamma_B(\frac{In2}{G})^{\frac{1}{2}}. \quad (2.7)$$

The amplification mechanism provided by SBS is distributed along the whole optical fibre and is renowned for its low threshold, high energy efficiency and narrow spectrum with an approximately 20-MHz bandwidth in the standard telecommunication fibre.

2.1.2 Gain provided by Stimulated Raman Scattering

Stimulated Raman scattering (SRS) is another important nonlinear effect in optical fibres. As the incident photon with energy $\hbar\omega_p$ is scattered from the optical phonon related to the transition of molecular vibrational states, the frequency of the scattered photon will be downshifted to ω_s known as the Stokes frequency exciting the molecule to a higher vibrational state or upshifted to ω_a known as the anti-Stokes frequency leaving the molecule in the ground state, which can be understood via using

the energy level diagrams shown in figure 2.1. Typically, the Stokes wave is much stronger than the anti-Stokes wave because the population of level *n* is smaller than that of level *g* in thermal equilibrium. Therefore, we mainly discuss the characteristics of Stokes wave. Even though the spontaneous Raman scattering is very weak, the intense pump light can induce the nonlinear phenomenon of SRS during which most of the pump energy is converted into the Stokes frequency and the Stokes components experience a rapid growth.

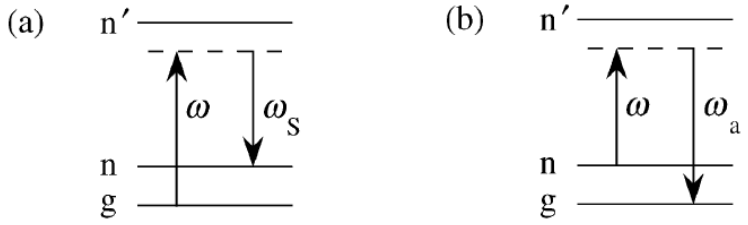

Figure 2.1 | Schematic illustration of (a) spontaneous Raman Stokes scattering and (b) spontaneous Raman anti-Stokes scattering from a quantum-mechanical viewpoint. (Figure from [11])

The non-crystalline nature of silica glass results in a continuum spread of molecular vibrational frequencies. As a result, the gain provided by SRS extends over a broad frequency range (up to 40 THz) with a broad peak located near 13 THz in optical fibres [12], as illustrated in figure 2.2, and optical fibres can work as broadband amplifiers. Though Raman gain suffers from its high threshold, its collaboration with Rayleigh scattering can open up the possibility of applications of random distributed feedback lasers in long-distance sensing system [5].

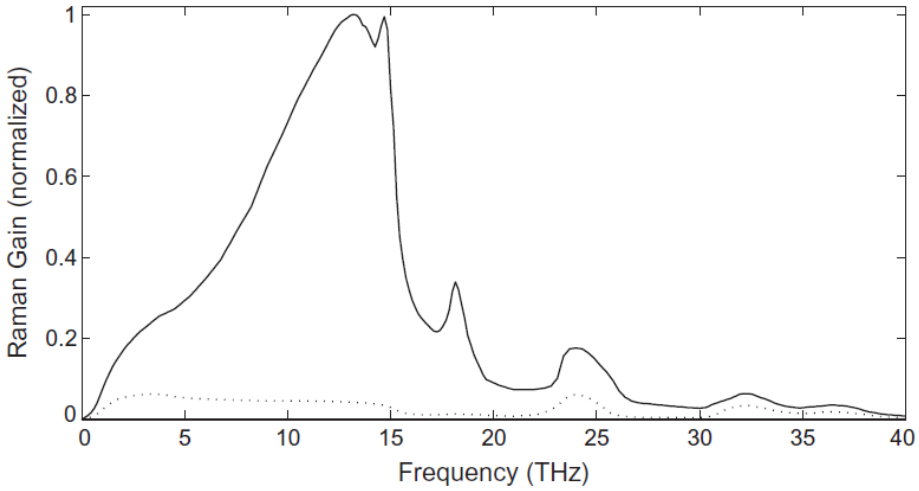

Figure 2.2 | Normalised Raman gain for fused silica when the pump and Stokes waves are co-polarised (solid curve). The dotted curve shows the situation in which the pump and Stokes waves are orthogonally polarised. (Figure from [12])

2.1.3 Gain provided by Erbium-doped fibres

Optical fibres doped with certain rare earth elements such as erbium can be used as the gain medium of a laser or optical amplifier. The erbium-doped fibre (EDF) plays a pivotal role in modern communication systems thanks to its high energy efficiency and broad gain bandwidth around the 1550 nm wavelength that coincides with the low-loss transmission band in infrared optical communications.

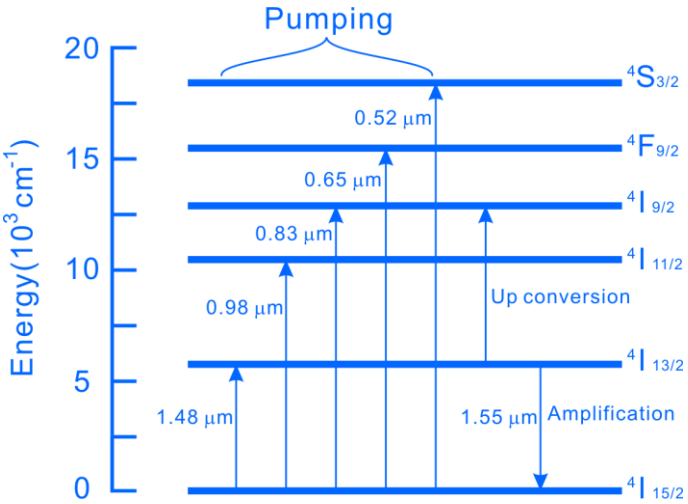

Figure 2.3 | Energy level diagram of the triply ionised erbium ion.

Erbium ions act as a quasi-three-level laser in the amplification of 1550-nm-

wavelength light, shown in figure 2.3 [13], including the ground state ($^4I_{15/2}$), the first excited state ($^4I_{13/2}$) and one of other higher excited states (i.e. $^4I_{11/2}$). The wavelength of pump light is usually selected in 980nm or 1480nm associated with the $^4I_{15/2}$ - $^4I_{13/2}$ transition and $^4I_{15/2}$ - $^4I_{11/2}$ transition, respectively, because of the pump excited-state absorption in other pump bands. Note that carriers occupy the excited state $^4I_{11/2}$ only about 1μs and then decay into the metastable state $^4I_{13/2}$ via the nonradiative transition, exciting molecules to higher vibrational states. So 1480 nm pumping is more efficient than 980 nm pumping because it avoids the non-radiative transition from $^4I_{15/2}$ to $^4I_{13/2}$. The incident photon in the 1550-nm-wavelength band can stimulate the excited erbium ion to emit a photon of exactly the same wavelength and phase as the incident photon, thus enabling the optical amplification. The inhomogenously broadened Stark-split levels of $^4I_{15/2}$ and $^4I_{13/2}$ leads to a truly broad gain spectrum, as shown figure 2.4. For the erbium-doped fibre random lasers, the assisted random feedback is provided by the accumulated Rayleigh feedback in the ultra-long optical fibre or the random gratings.

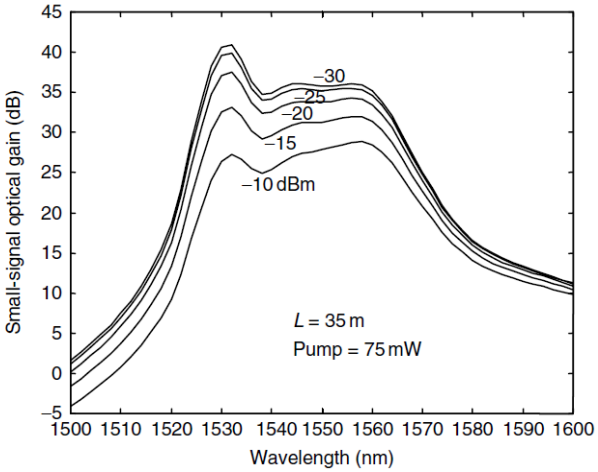

Figure 2.4 | Example of EDF amplifier optical gain versus wavelength at different input optical signal power levels. (Figure from [14])

2.2 Feedback Mechanisms in Optical Fibres

There are two regular feedback mechanisms in fixed-cavity fibre laser including the optical fibre coupler and the fibre Bragg gratings. Within the resonator of a fibre laser, a dichroic fibre coupler can be used to inject pump light, and another fibre coupler can be used as the output coupler. This technique is used particularly in fibre ring lasers. A Fibre Bragg grating consists of a periodic modulation of the refractive index in the core of an optical fibre. Light guided along the core of an optical fibre will be scattered by each grating plane and the Bragg condition decides the reflectivity spectrum. Fibre Bragg gratings can be used as end mirrors of fibre resonator and also restrict the reflection to a very narrow spectral range. In this section, we focus on the characteristics of feedback mechanisms in random fibre lasers.

2.2.1 Rayleigh Scattering

Rayleigh scattering is an essential loss mechanism initiated by scattering of light from fluctuations of thermodynamic quantities such as entropy, density, or temperature [11]. It is a type of elastic scattering and does not induce any frequency shift. In the high-quality telecommunication fibre, the uniform distribution of the refractive index irregularities supports a large ensemble of Rayleigh reflectors with the weak reflection coefficient $r \approx 7.3 \times 10^{-8}$ m^{-1} along the whole fibre. Fortunately, the intrinsic waveguide structure of optical fibres can facilitate the accumulative effect of backscattered photons in spite of such small r.

Random fibre lasers based on the Rayleigh feedback can be thought of a linear

coupling of numerous Fabry-Pérot cavities provided that the optical fibre nonlinearities are ignored. As a result, fixed resonance properties never appear. A large number of densely spaced Rayleigh mirrors leads to a considerable number of resonant modes with an extremely small free spectral range between adjacent modes, and the temporal dependence of the random supposition of elementary cavities also results in the strong mode-hopping which could be aggravated by the local heat exchange with the surrounding environment. Therefore, the Rayleigh feedback based random fibre laser is pseudo-continuously mode-less [15], shown in figure 2.5.

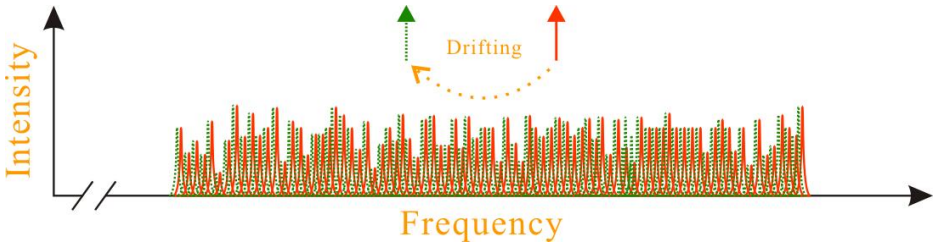

Figure 2.5 | Pseudo-continuously mode-less optical spectra.

2.2.2 Random Gratings

Rayleigh feedback based random fibre lasers suffers from the long fibre lengths and the strong mode-hopping due to a large density of random modes. Thus, an alternative random feedback mechanism in a compact size is needed. Random gratings have achieved this task. The array of randomly spaced gratings could be written in the core of an active fibre (e.g. EDF) by using intense ultraviolet laser and act as strong scattering centers forming the random feedback [16, 17]. The femtosecond laser micromachining can also achieve the high-precision deep refractive index modulation in the passive fibre by the multi-photon absorption process with femtosecond laser

pulses at 800 nm, and these randomly distributed reflectors with much higher reflectivity result in a discrete set of interference peaks with random spectral separations and varying quality factors [18].

2.3 Classical Structures of Random Fibre Lasers

2.3.1 Random Brillouin Fibre Lasers

The first study of SBS based fibre lasers with distributed Rayleigh feedback has been explored in the pulsed regime [19], where a 300-m non-uniform single-mode fibre was chosen as the open laser cavity. As the power of the pump light is well above the SBS threshold, SBS Stokes waves were created and double Rayleigh scattered Stokes waves worked as the seed of new SBS amplification processes. As the SBS amplification compensated for the loss, this system started to lase. Arbitrary two distributed Rayleigh mirrors can form a Fabry-Pérot resonator and the output can be considered as the superposition of multitudinous resonance curves, leading to the strong colour-selectivity and the laser linewidth of ~100 kHz.

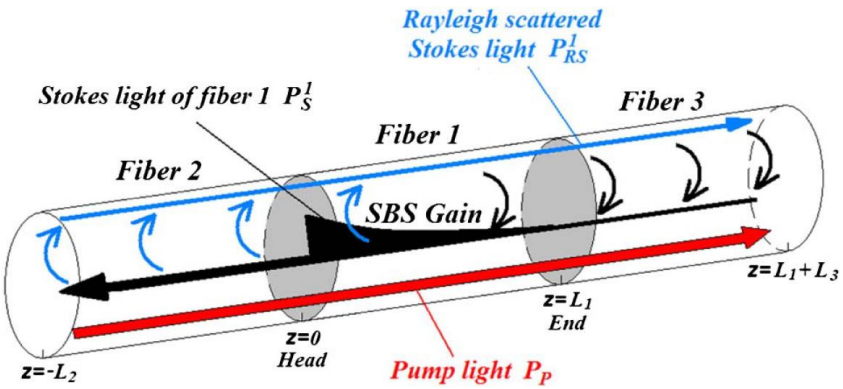

Figure 2.6 | Cascaded fibre composed of three types of fibres with different Brillouin

frequencies. (Figure from [20])

Nowadays, the optical fibre has been manufactured to have a low loss (~0.2dB/km near 1.55μm) leading to a much smaller Rayleigh coefficient and so the aforementioned random-lasing scheme cannot work in modern telecommunication fibres. In the usage of low-loss optical fibres, a scheme of the Brillouin-gain based random fibre laser operating in the continuous-wave (CW) regime was developed by Pang *et al.* as illustrated in figure 2.6 [20]. The random laser was pumped from one side and consisted of three different fibre spans which were spliced together. The Rayleigh scattering of the SBS Stokes light generated by the middle fibre span was enhanced by other two fibre spans. After the Brillouin gain, provided by the middle fibre, was high enough to compensate the effective loss of the SBS Stokes light in a roundtrip, the random lasing emission with a linewidth of ~3.4 kHz was observed. However, the lengths of Rayleigh feedback fibres limited the effective reflection, leading to the low lasing efficiency and only 20-dB contrast. In chapter 4, the dual-pumping approach was used to guarantee an efficient round-trip amplification and improve the lasing efficiency.

2.3.2 Random Raman Fibre Lasers

In 2010, Turitsyn *et al.* reported an important breakthrough in the stable CW lasing of the near-Gaussian beam at 1550 nm in a 83-km-long standard telecommunications fibre through using only homogeneously distributed Raman amplification and Rayleigh distributed feedback, without any additional reflectors, as shown in figure 2.7 [5]. As the pump power is well above the lasing threshold, the laser starts to

strongly suppress self-pulsation and is free from the chaotic optical spectrum. Eventually, the oscillation narrows continuously towards two pronounced peaks localised near the Raman gain maxima, yielding efficient lasing in both spectral and temporal domains. This laser scheme opens a new research direction in the stationary random distributed feedback fibre laser and is also promising for various applications like remote sensing.

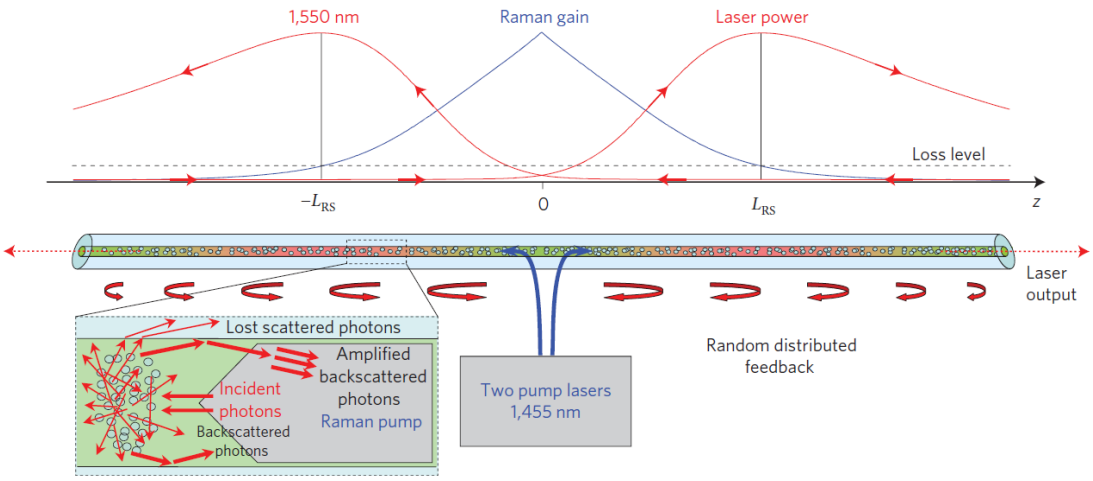

Figure 2.7 | Principle of random distributed feedback fibre laser operation. (Figure from [5])

2.3.3 EDF-Gain based Random Fibre Lasers

A semi-open random Fabry-Pérot resonator was introduced by our group in which the EDF was enclosed by a fibre Bragg grating (FBG) reflecting a narrow wavelength band with a center wavelength of 1539.4 nm and 3 dB bandwidth of 0.03nm from the broad amplified spontaneous emission of the EDF and a ultra-long optical fibre that supplied the random distributed feedback and suppressed the thermal frequency noise at higher frequencies [21]. Later, the eight-segment random gratings was incorporated into a fibre ring laser configuration, where an erbium-doped fibre amplifier (EDFA)

provides a broadband gain spectrum and an optical band-pass filter (OBPF) with 3-GHz bandwidth serves for wavelength locking and spectral filtering. These side-written photoinduced strong scattering planes provided the random feedback and acted as numerous low-finesse spectral filters, ensuring a narrow lasing envelope with the linewidth of 2.1 kHz [18].

With the aforementioned literature review, we are now ready to discuss the schematics and lasing mechanisms for designed novel random Brillouin fibre lasers.

2.4 Resonance Properties of Random Brillouin Fibre Lasers

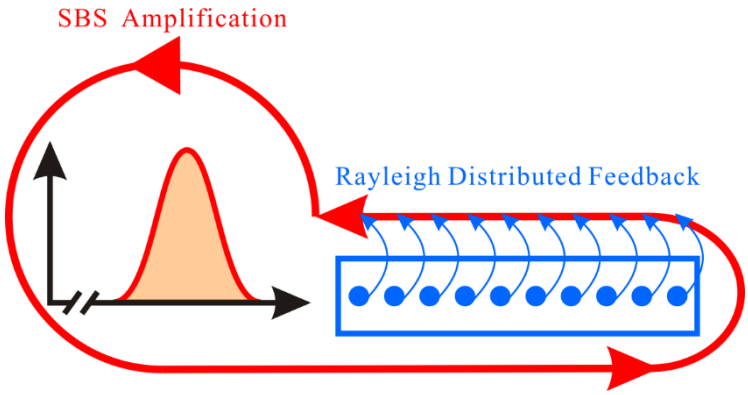

Figure 2.8 | The typical schematic of RBFL.

The random Brillouin fibre laser is constituted of the efficient Brillouin amplification and the accumulated Rayleigh distributed feedback, as shown in figure 2.8, and can be usually studied using two-model systems. The first model considers the gain and the random feedback supplied by different optical fibres. This is the case for our random fibre ring resonator and more details will be discussed in Chapter 3. In the second model system, the random feedback mechanism can be provided by the Brillouin gain fibre itself, such as our random fibre Fabry-Pérot (FP) resonator with a full

description in Chapter 4. In this section, we mainly focus on the resonance property of the random fibre ring laser.

Conventional optical ring resonators are made of a closed loop waveguide with a fixed cavity length, leading to a periodic interference pattern in spectra, while random fibre ring lasers are composed of a circulated gain mechanism and the "Rayleigh mirror clouds". The resonant feedback in this random fibre ring resonator is achieved by the refractive index irregularities distributed along the whole Rayleigh scattering feedback (RSF) fibre, and the build-up of radiation in this random laser is determined by the complex yet completely coherent scattering in the RSF fibre and the round-trips amplification in the gain fibre. Note that coherent scattering means that scattered waves can finish the field superposition, while incoherent scattering represents the intensity superposition. The cavity length L_{Ray} is not constant for this random fibre resonator and follows a random process statistically with the expected value L_0 and the standard deviation σ_L. Physically, this means that the lucky photons captured in this open cavity follow complex and various trajectories, conducting a random walk in the round-trip phase shift of the optical wavelets and then a unique interference effect. Therefore, the laser characteristics of this kind of resonator have non-periodic interference patterns in optical spectrum due to a random distribution of the optical path length for arbitrary Rayleigh-scattered Stokes light, leading to the randomly resonant properties inside the SBS gain envelope. If the polarization effect and the phase noise terms are omitted, the optical field emitted from the output port is given by

$$E_{out} = \sum_{m=1}^{M} E_S \prod_{u=1}^{m} \sum_{k=1}^{N} e^{-\frac{\alpha}{2} L_{Ray,u(k)}} e^{G_{u(k)}} r_{u(k)} e^{-i2\pi \frac{\nu}{c} n L_{Ray,u(k)}} \tag{2.8}$$

where $L_{Ray,u(k)}$ is the optical path length of photons scattered from k-th Rayleigh scattering center in the u-th pass; α and n are the mean loss coefficient and refractive index respectively; $\exp(G_{u(k)})$ and $r_{u(k)}$ are the SBS amplification coefficient and the distributed Rayleigh reflection coefficient for photons scattered from k-th Rayleigh scattering center in the u-th pass, respectively; ν is the optical frequency and c is the photon velocity in vacuum.

Figure 2.9 shows a numerically simulated spectral information of a combination of SBS Stokes light scattered from 1000 Rayleigh scattering centers along the 10-km RSF fibre with different amplifying round-trips. Note that the uncertainty of the cavity length twice as the RSF fibre length is comparable to that of 25-km gain fibre. The simulated spectrum exhibits a chaotic interference pattern and the resonant lasing components appear at stochastic positions, indicating the random fibre ring laser operates in the pseudo-continuous modeless state. As an unflattened SBS gain profile is adopted, the resonant lasing spikes would preferably occur in the frequency region where the Brillouin gain could overcome the total cavity loss, leading to the generation of random lasing behavior and an overall narrowing of the emission spectrum.

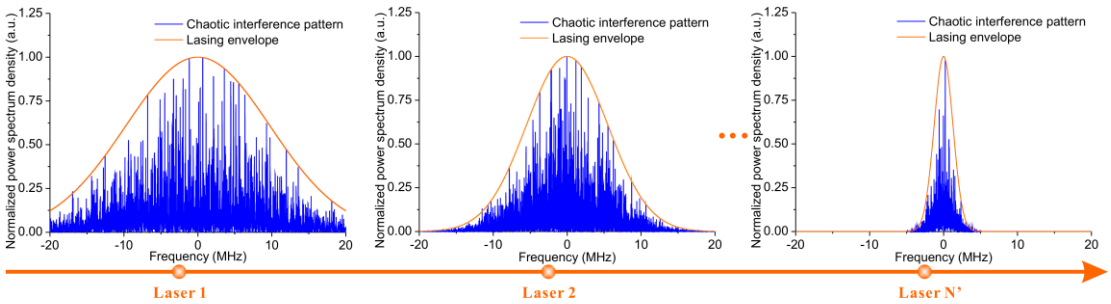

Figure 2.9 | The simulated chaotic interference pattern in optical spectra (zero frequency corresponds to 1.3×10^{14} Hz).

The following is an additionally qualitative description for characteristics of the random fibre laser. The formation of such a narrow lasing envelope of laser *N'* in figure 2.9 requires that the favored spectral components must maintain the resonant feedback advantage in the whole build-up process and suppress other individual components within the SBS gain envelope by gain depletion. This condition is easy to achieve in the conventional laser thanks to its stability in phase, while this is a completely different case in the random fibre ring laser with a large standard deviation of the photon path-length distribution. Firstly, the Rayleigh random laser operates in a pseudo-continuous mode-less state, because the extremely large number of Rayleigh scattering centers in the ultra-long optical fibre brings out a very short mean free spectral range between adjacent resonance modes. Not only the presence of temporal perturbations of Rayleigh scattering due to the local heat exchange with the surrounding environment but also the arbitrary distribution of scattering centers can force any mode to drift away from its initial position and overlap with adjacent ones. Moreover, as the resonant photons are launched into the RSF fibre, most of them will leak out of the random fibre ring resonator and only Q≈1/600 [19] of Rayleigh scattered photons are backscattered randomly in space and guided by the optical

waveguide with arbitrary phase. As a consequence, resonant photons will lose the priority in the following gain competition and they cannot get sufficient amplification for a long time, which makes the narrow emission output hard to appear in this random fibre ring laser. The SBS mechanism is also not stable along the whole 25-km gain fibre due to external disturbances and material non-uniformities, which could affect the phase of resonant waves and disturb the build-up of narrow-band emission.

The random laser may be regarded as the incoherent superposition of a multitude of elementary lasers with different weights determined by how much energy of pump is assigned to different sub-lasers, shown in Eq. (2.9):

$$S_{E,net}(\omega) = \sum_{k=1}^{N'} A_k S_{E,k}(\omega) \tag{2.9}$$

where A_k and $S_{E,k}(\omega)$ are the weight and the field spectrum of sub-laser k, respectively. It is worth noting that all the elementary lasers operate in unstable regions where their resonant features are susceptible and they could easily switch to other operation modes. The experimental result indicates that sub-laser 1 or 2 in Fig. 2.9 dominates in the random fibre ring laser, but narrow random-lasing radiation can occur in the random fibre FP resonator thanks to not only its small standard deviation of the photon path-lengths but also its significant round-trip amplification offered by the designated dual-pumping approach.

Chapter 3

Generation of ultra-narrow linewidth microwave signals based on random Brillouin fibre laser

Nowadays there is an increasing interest in the exploration of microwave sources generating widely tunable pure signals for a multitude of applications in the information and communication technology. This chapter presents a novel random Brillouin fibre laser scheme that stimulated Brillouin scattering provides an effective amplification mechanism and Rayleigh scattering along an ultra-long standard telecommunication optical fibre supplies random distributed feedback. The high degree of mutual coherence between two Stokes beams as well as the random phase noise evolution leads to the generation of ultra-narrow linewidth microwave signals with a Dirac delta function profile. This will revolutionise the design and construction of microwave sources and pave the way for random laser based terahertz generation and applications.

3.1 Introduction

High spectral purity microwave sources are very valuable in a multitude of applications, such as high speed optoelectronics characterizations [22], telecommunications [23], phased-array radars [24], and remote distributed antenna

systems [25]. A straightforward method of generating microwave signals is to use optically heterodyne detection of either two independent lasers [26] with required frequency difference or dual-frequency outputs of a single laser [27, 28]. The first approach is competitive in its flexibility of frequency control despite its obvious drawback that the linewidth and frequency drifting of two lasers are directly transferred to the generated microwave signals. In the second approach, noise mechanism originating with the conventional laser cavity could be mostly cancelled out thanks to the common cavity and gain shared by two resonance modes at the cost of limited tuning frequencies of the two independent lasers, however there is a potential problem of the gain competition. Fortunately, Brillouin fibre lasers, renowned for their inherent features of spectral stability and narrow gain profiles, are excellent candidates to avoid such mode competition and have been widely used in the generation of high-quality microwave sources [29-32]. Furthermore stimulated Brillouin scattering (SBS) can work as an optical filter to selectively amplify sidebands in microwave signal generation [33].

Here, we propose and experimentally demonstrate, for the first time, a novel approach to efficiently generate ultra-narrow microwave signals by using a random Brillouin fibre laser scheme with Brillouin gain and Rayleigh feedback. Based on the synchronization of optical modes from two optical signals with random phase accumulated over an ultra-long optical fibre, a high degree of mutual coherence between two initially non-coherent Stokes signals is generated, resulting in a beat signal up to 23 GHz with 20-dB linewidth of ~1 kHz and 70-dB contrast

corresponding to a Dirac delta function profile.

3.2 Theoretical Model

3.2.1 Laser Characteristics

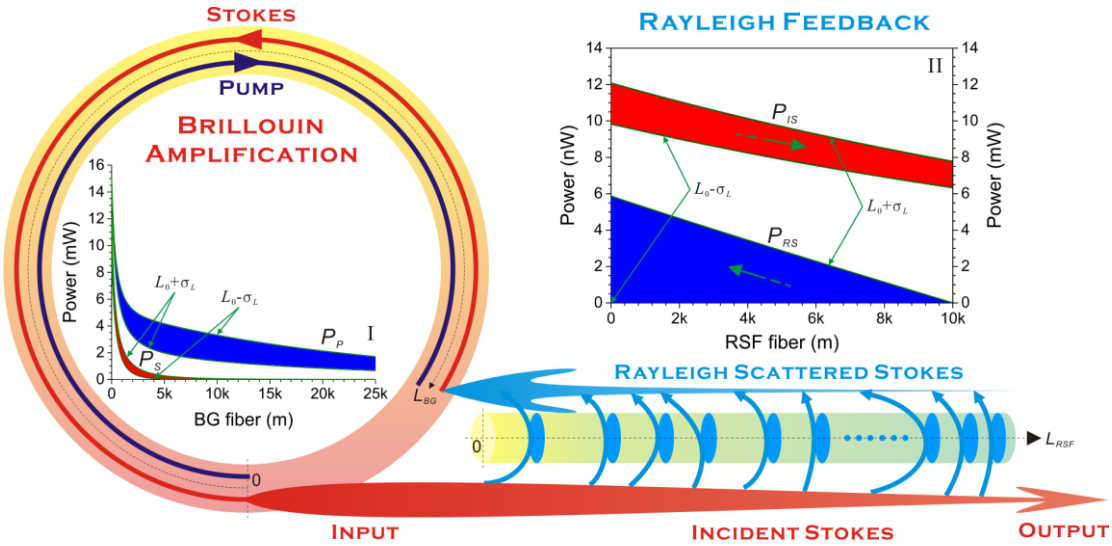

Figure 3.1 | Illustration of a random Brillouin fibre laser configuration; simulated power evolution of (I) pump and Stokes light in the BG fibre and (II) incident Stokes light and Rayleigh scattered Stokes light in the RSF fibre.

Figure 3.1 presents the random Brillouin fibre laser configuration consisting of SBS gain and Rayleigh feedback. Pump light launched into the Brillouin gain (BG) fibre leads to the SBS process, generating inelastically backscattered Stokes light with a frequency downshift Ω_B with respect to the pump light due to the Doppler effect. The Stokes light enters into the Rayleigh scattering feedback (RSF) fibre with a large ensemble of scattering centers, and the reinjection of Rayleigh backscattered Stokes light into the BG fibre provides dynamic distributed feedback in the Brillouin amplification process, forming a random fibre ring laser. In the quasi-stationary regime, the power evolution of the pump and Stokes light, P_P and P_S, in the BG fibre as well as the incident Stokes light and Rayleigh scattered Stokes light, P_{IS} and P_{RS}, in

the RSF fibre can be expressed by

$$\begin{cases} \partial P_P / \partial z_1 = -g_B P_P P_S - \alpha P_P \\ \partial P_S / \partial z_1 = -g_B P_S P_P + \alpha P_S \\ \partial P_{IS} / \partial z_2 = r P_{RS} - \alpha P_{IS} \\ \partial P_{RS} / \partial z_2 = -r P_{IS} + \alpha P_{RS} \end{cases} \tag{3.1}$$

where z_1 and z_2 are the positions in the BG fibre with a length of L_{BG} = 25 km and the RSF fibre with a length of L_{RSF} = 10 km, respectively; g_B is the Brillouin gain coefficient, g_B = 0.21 $m^{-1}W^{-1}$; α is the linear loss coefficient, $\alpha = 4.4\times10^{-5}$ m^{-1}; r is the Rayleigh reflection coefficient, $r = 7.3\times10^{-8}$ m^{-1}. The continuity of the SBS Stokes power between the BG fibre and the RSF fibre within the random laser gives the boundary conditions: $P_S(z_1=0) = P_{IS}(z_2=0)$ and $P_S(z_1=L_{BG}) = P_{RS}(z_2=0)$. The Brillouin gain factor $G = g_B P_P(z_1=0) L_{BG}$ is well above the SBS threshold, i.e. $P_P(z_1=0)$ = 15 mW. Photons travel in the open cavity following complex trajectories since the cavity reflectivity is so low that the variable cavity length follows a statistical distribution with the expected value $L_0 = L_{BG} + L_{RSF}$ and the variance $\sigma_L = L_{RSF}$. Figure 3.1-I shows that P_S experiences exponential growth over an effective amplification length that is reduced to a few kilometers due to pump depletion, and blue and red regions respectively correspond to the pump and Stokes power fluctuations arising from the feedback dynamics. Figure 3.1-II shows that P_{RS} accumulates in the direction back to the BG fibre while P_{IS} drops along the RSF fibre owing to the linear loss, and the coloured regions denote the power fluctuations, indicating the random Brillouin fibre laser output power fluctuations ranging from 6.3 mW to 7.8 mW.

The highly pump-depleted SBS could cause a certain reduction in the effective

SBS amplification time and chaotic intensity fluctuations [10], while the SBS mechanism even in high pumping level would become temporally more unstable because the Rayleigh feedback provides the accumulative effect for the phase of optical wavelets and promotes the dynamical emission. Rayleigh backscattering is an essential loss mechanism initiated by scattering of light from fluctuations of thermodynamic quantities [11] and it creates time-delayed phase variations in optical waves because of spatial and temporal perturbations in the local refractive index of the optical fibre. Therefore, time derivatives in equation (3.1) cannot be neglected for such a non-steady state, leading to a more comprehensive description of the random Brillouin fibre laser dynamics.

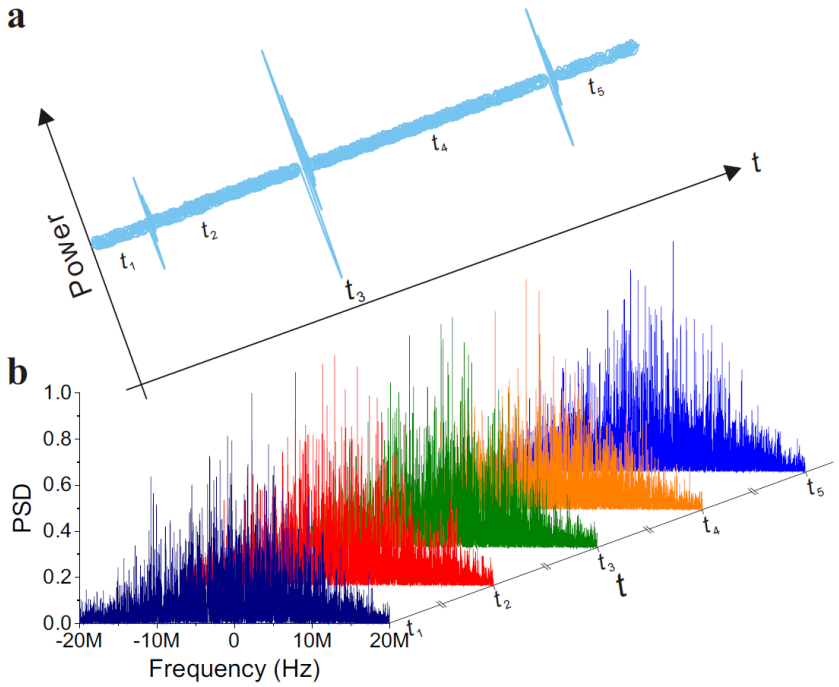

Figure 3.2 | Simulated chaotic emission spectrum evolution occurring over time in an unsteady state (zero frequency ~ 1.3×10^{14} Hz).

As illustrated in Figure 3.2a, the quasi-stationary amplification process (t_1, t_2, t_4, t_5) dominated by the thermally induced dynamic phase shifts would cause the chaotic

Stokes power fluctuations – floating pulses. The strong pump-Stokes interaction gives rise to acoustic pressure waves, and the creation and decay of the pressure wave occur over the phonon lifetime of silica $\tau_{phonon} \approx 10$ ns. Since the power spectral density (PSD) of the thermal noise throughout its frequency spectrum is restrained by the finite bandwidth of the SBS gain, the chaotic oscillation period of the Stokes power could be very short approaching τ_{phonon}. Thus, although the continuous wave (CW) pump light is delivered through the BG fibre, the floating Stokes pulses with nanosecond-level pulse duration actually return from the RSF fibre, and the energy exchange between the CW pump and Stokes pulses completes within an extremely short timeframe. Furthermore, the abrupt bursts of large transmission attenuation (t_3) that causes a series of damped relaxation oscillations of the Stokes power, suffering from the random and unpredictable cavity loss owing to either polarization-dependent loss as the optical fibre is treated by using a wave-plate model or structural vibrations induced by unwanted acoustic waves with relative high loss factors, as well as the nonlinear refraction effect [34].

The SBS process occurs over a distribution of frequencies about the central Brillouin frequency ν_B due to different line-broadening mechanisms while the large pump depletion as well as the Stokes pulse interactions with the pump eventually yields particular bandwidth $\Delta\nu_B$ in the corresponding Brillouin gain spectrum $S(f)$. The time-dependent Brillouin gain spectrum exhibits an intermittent reshaping of the emission spectrum containing all frequency components of the pulsed Stokes light. The Rayleigh scattering centers in the ultra-long RSF fibre bring a large number of

resonance modes and very short mean free spectral ranges between adjacent ones, and the presence of temporal perturbations of Rayleigh scattering results in strong mode coupling by forcing resonance modes to drift away and overlap with each other. Figure 3.2b shows the numerically simulated spectral information of the SBS Stokes light scattered from a total number of k = 1000 randomly distributed Rayleigh scattering centers along the 10 km RSF fibre. The instantaneous spectrum determined by the Brillouin gain with specific bandwidth (e.g. $\Delta\nu_B \approx 20$ MHz) exhibits a non-periodic interference pattern, that is, the stochastic resonant lasing spikes preferably appear in frequency regions where the Brillouin gain could overcome the total cavity loss. Noticeably, this random fibre ring laser operates under severe mode-hopping and mode-competition conditions which is actually a modeless state [15]. So the emission spectra are pseudo-continuous. Specifically, the favored spectral components near the maximum of the Brillouin gain spectrum and the suppression of other frequency components by gain depletion would not be continuously sustained in the overall lasing process since the resonant feedback conditions can be easily varied by the great uncertainty of photon paths and ineluctable external perturbations. Furthermore, when the resonant light is launched into the RSF fibre, only a small fraction of the randomly backscattered light can be maintained and guided through the random fibre ring resonator with arbitrary phase. As a consequence, the narrow-band emission spectrum is impossible to be persistently observed as the successive beams of backscattered light cannot superpose constructively in subsequent gain competition processes. In addition, occasional lasing of narrow-band spectral component transfers energy to

lower-frequency ones in the cascaded Brillouin process to further aggravate instability [35].

3.2.2 Principle of High-purity Microwave Signal Generation

The chaotic lasing process can be statistically described by the phase noise from thermal fluctuations that follows a Gaussian amplitude distribution. The backscattered light at the input end of the RSF fibre is a summation of all Stokes waves from k Rayleigh scattering centers and the accumulated random phase noise adds up over the RSF fibre by the number of passes $m \approx |1\text{-}rL_{eff}e^{Geff}|^{-1}$, where L_{eff} is the effective RSF fibre length and G_{eff} is the effective Brillouin gain factor, and both values are strongly relying on the external feedback conditions. The nonlinear amplification of Stokes light in SBS is significant to compensate for small reflection coefficients of the distributed Rayleigh mirrors. The unique configuration of connecting both ends of the BG fibre to the input end of the RSF fibre guarantees a continuous transmission of the phase information with an infinite round-trip number. The major mechanism behind the high degree of mutual coherence between the two Stokes beams A and B and the generation of a Dirac-profile spike is the synchronous evolution of the averaged random phase noise. The optical field in the m-th pass through the RSF fibre where the intense thermal effect aggravates can be written as

$$\begin{aligned} E_{\text{out},m} &= E_{\text{in}} e^{i\phi_0} e^{-\alpha L_{RSF}} \sum_{k=1}^{N} r_0 e^{G} e^{-\alpha \tau_{k,m} c/n} e^{i\phi_{k,m}(t-\tau_{k,m})} \\ &\approx E_{\text{in}} e^{i\phi_0} e^{-\alpha L_{RSF}} r_0 a e^{G} e^{i\phi_m(t)}, \end{aligned} \tag{3.2}$$

with

$$a=\sum_{k=1}^{N}e^{-\alpha\tau_{k,m}c/n};\qquad \phi_m(t)=\frac{\sum_{k=1}^{N}e^{-\alpha\tau_{k,m}c/n}\phi_{k,m}(t-\tau_{k,m})}{\sum_{k=1}^{N}e^{-\alpha\tau_{k,m}c/n}}\approx\frac{\sum_{k=1}^{N}\phi_{k,m}(t-\tau_{k,m})}{N},\ N\to\infty,$$

where E_{in} is the quasi-monochromatic Stokes field rising from the noise in both the SBS and random feedback mechanism; ϕ_0 is the initial phase; α is the mean attenuation coefficient; r_0 is the backscattering amplitude; $\phi_{k,m}(t-\tau_{k,m})$ is the uniform distributed phase contribution for the k-th Rayleigh scattering center in the m-th pass through the RSF fibre; $\tau_{k,m}$ is the corresponding delay time; $\phi_m(t)$ is the weighted-average phase noise. Although the thermal fluctuation induced phase change on any individual Rayleigh scattering center could vary in a large range in the presence of the long optical fibre, the first-order Taylor series approximation is still valid because instantaneous changes in the thermodynamic properties of the Rayleigh scattering centers result in the relative small $\phi_{k,m}$. Since the backscattering amplitude r_0 is associated with every scattering center, $r_0 a \approx rL_{eff}$ and $r_0 a e^G$ is approaching to 1 as m increases to infinity under consideration of an innumerable amount of scattering centers. The optical field from the output end of the RSF fibre is the summation of optical fields with different round-trip numbers

$$E_{\text{out}}=\sum_{m=1}^{M}E_{\text{out},m}=E_{\text{in}}e^{i\phi_0}e^{-\alpha L_{RSF}}\sum_{m=1}^{M}r_0 a e^{G}e^{i\phi_m(t)}\approx E_{\text{in}}e^{i\phi_0}e^{-\alpha L_{RSF}}be^{i\Phi(t)},\tag{3.3}$$

with

$$b=\sum_{m=1}^{M}r_0 a e^{G};\qquad \Phi(t)=\frac{\sum_{m=1}^{M}r_0 a e^{G}\phi_m(t)}{\sum_{m=1}^{M}r_0 a e^{G}}\approx\frac{\sum_{m=1}^{M}\phi_m(t)}{M}=\frac{\sum_{m=1}^{M}\sum_{k=1}^{N}\phi_{k,m}(t-\tau_{k,m})}{M\times N},\ M(N)\to\infty.$$

The degree of mutual coherence between two Stokes beams A and B can be

defined as

$$\gamma_{AB} = \frac{1}{\tau_D}\int_0^{\tau_D} e^{i(\Phi_A(t)-\Phi_B(t))}dt = \left\langle e^{i(\Phi_A(t)-\Phi_B(t))} \right\rangle = |\gamma_{AB}|e^{i\theta}, \quad (3.4)$$

where τ_D is the characteristic time constant of the detection system [36]; Φ_A and Φ_B are the overall phase noise of output signals from *A* and *B*, respectively; the angle brackets indicate time averaging; θ is a real constant. Figure 3.3 illustrates how Φ_A and Φ_B evolve to enhance γ_{AB} with the rising length of the RSF fibre L_{RSF}. As illustrated in Figure 3.3a, the yellow background colour represents the weighted-average phase noise ϕ_m in the range between $-\pi$ and π in the *m*-th pass through the RSF fibre, and the blue curve represents the probability density function (PDF) of the phase noise over the RSF fibre including all the Rayleigh scattering centers. The distribution of all the possible values of the random phase noise for a single Rayleigh scattering center (k = 1) has a constant probability, while the PDF of the average phase noise for multiple single Rayleigh scattering centers ($k = N$) can be represented by a normal distribution, and it continuously develops to a Dirac delta function for the limit $k\rightarrow\infty$ even though it is practically unattainable because of the limit of the intrinsic loss mechanism due to Rayleigh scattering and the finite gain coefficient. In Figure 3.3b, the pink background colour represents the overall phase noise $\Phi_{A(B)}$ after *m* passes through the RSF fibre, and the blue curve represents the PDF of the further reduced phase noise. It is noted that the number of passes *m* may be constantly reset to zero as tremendous loss takes place in the open cavity to discontinue the light propagation from the RSF fibre back to the BG fibre so that the PDF of the overall

phase noise will not develop to a Dirac delta function for the limit $m \to \infty$. In Figure 3.3c, the red and green regions represent the ensemble of the instant phase noise for A and B, respectively. It is obvious that Φ_A and Φ_B have an indefinite phase relationship under the minimum values of k and m. However, the overall difference in the phase noise between A and B for the limit $k \to \infty$ and $m \to \infty$ would be reduced to a fixed value depending on the initial phase ϕ_0 because there is a very high probability that the phase noise over all the Rayleigh scattering centers falls in the range close to the expectation of the normal distribution with the mean of zero, leading to continuously increased degree of similarity. In practice, m relies not only on the pumping level but also on the external feedback condition, and k is associated with the fibre length.

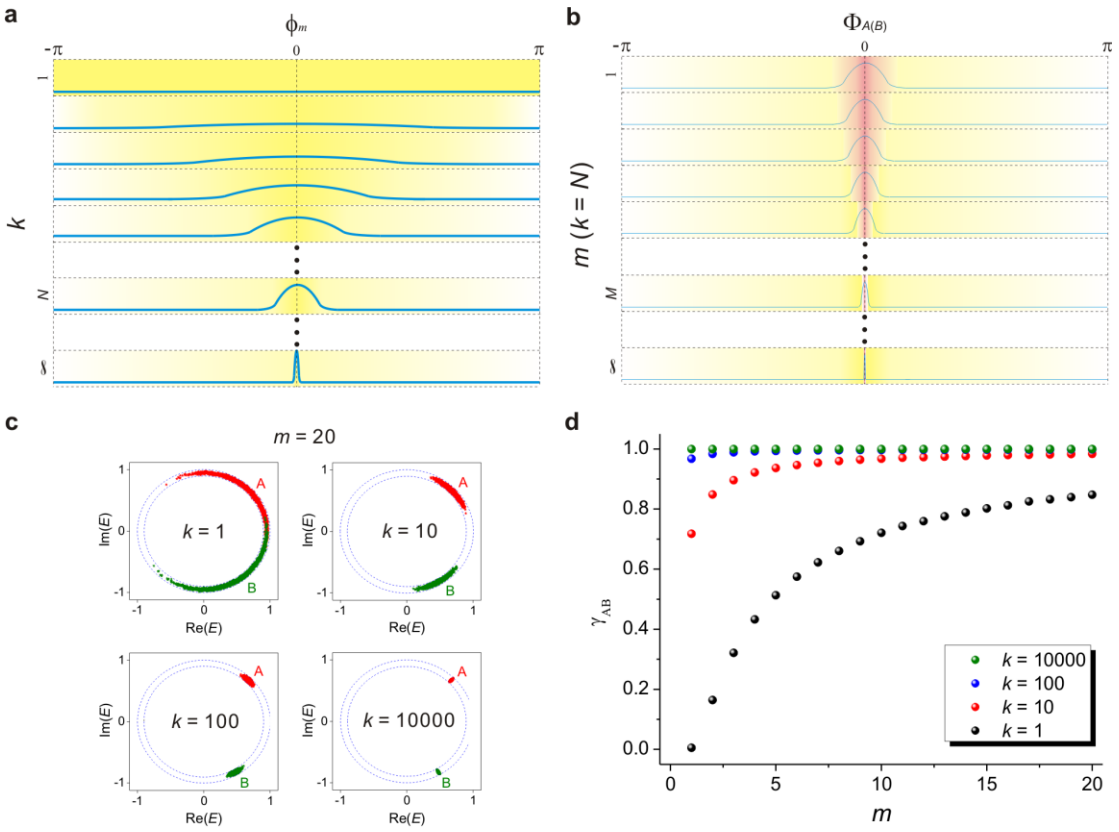

Figure 3.3 | **a, b,** Illustration of random phase noise synchronization process between two optical beams. **c,** Phase-space plot of two Stokes beams A and B with k = 1, 10, 100, 10000 and the same m = 20. **d,** Simulated γ_{AB} as a function of m for k = 1, 10, 100, 10000.

The resultant optical field can be expressed as

$$E(t) = \sqrt{P_0} e^{i\left[(\omega_0 - \Omega)t + \Phi_A(t)\right]} + \rho\sqrt{P_0} e^{i\left[\omega_0 t + \Phi_B(t)\right]}, \tag{3.5}$$

where P_0 is the optical power in one beam and ρ is the power splitting ratio between the two beams; ω_0 is the optical frequency and Ω is the frequency difference. The photocurrent correlation function is given by equation (3.6), where the first term corresponds to the shot noise and the second term includes DC signals and mixing components [37, 38].

$$R_I(\tau) = qRG_E^{(1)}(0)\delta(\tau) + R^2 G_E^{(2)}(\tau), \tag{3.6}$$

with

$$G_E^{(1)}(0) = \left\langle E(t)E^*(t+\tau)\right\rangle,$$

and

$$\begin{aligned} G_E^{(2)}(\tau) &= \left\langle E(t)E^*(t)E(t+\tau)E^*(t+\tau)\right\rangle \\ &\approx \left(1+a^2\right)P_0^2 + 2a^2P_0^2\cos\left(\Omega\tau\right)\left|\gamma_{AB}\right|^2 e^{i2\theta} \\ &\quad + 2a^2P_0^2\cos\left(\Omega\tau\right)\left|\gamma_{AB}\right|^2 e^{i2\theta}\left\langle\left[\Phi_A(t+\tau) - \Phi_B(t+\tau)\right]\cdot\left[\Phi_A(t) - \Phi_B(t)\right]\right\rangle, \end{aligned}$$

where q is the electron charge; R is the detector sensitivity; $\delta(\tau)$ is the Dirac delta function; $\langle\exp(\pm ix)\rangle = \exp(-\langle x^2\rangle/2)$, as x follows a Gaussian probability distribution [39]. The second term corresponds to the mutual coherence in the PSD of the beat signal between A and B, and the corresponding photocurrent correlation function can be expressed as $R_{I\text{-co}}(\tau) = 2\rho^2R^2P_0^2|\gamma_{AB}|^2\exp(i2\theta)\cos(\Omega\tau)$. By using the Wiener-Khintchine theorem $S_{I\text{-co}}(f) = \mathcal{F}[R_{I\text{-co}}(\tau)]$, the PSD is obtained

$$S_{I\text{-co}}(f) = 2\pi\rho^2R^2P_0^2\left|\gamma_{AB}\right|^2 e^{i2\theta}\left[\delta(f-\Omega) + \delta(f+\Omega)\right]. \tag{3.7}$$

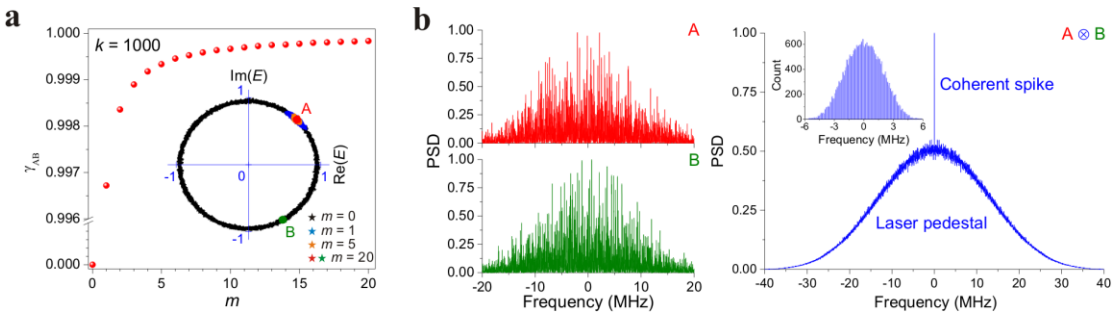

Figure 3.4 | **a,** Simulated γ_{AB} as a function of m for k = 1000. Inset is the phase-space plot of two Stokes beams A (m = 0, 1, 5, 20) and B (m = 20). **b,** Illustration of the algorithm embedded in optical process for generating an ultra-narrow microwave signal. A and B are the Brillouin gain spectra of two Stokes beams. ⊗ symbolises convolution. Inset is the simulated coherent spike frequency jitter statistics.

Figure 3.4a shows the simulated γ_{AB} as a function of m with k = 1000, and the inset of Fig. 3.4a implies that the boundary of the phase space of A or B is determined by the Stokes power fluctuations as well as the values of k and m. Experiencing a fast rising process, the DMC would come to 1 theoretically for the limit $k \to \infty$ and $m \to \infty$. As shown in Figure 3.4b, there exists a coherent spike on top of the random laser pedestal in the PSD of the beat signal between A and B. The increasing γ_{AB} brought by the RSF fibre functions for all spectral components within the pseudo-monochromatic spectrum. Because the contrast of the Dirac delta function in PSD is proportional to optical power, the coherent spike occurs around the central frequency of the electrical spectrum of the beat signal and the frequency drifts within a few MHz and the simulated frequency jitters of the coherent spike within a few MHz range is shown in the inset of Figure 3.4b-II. It is an intrinsic property of the Rayleigh scattering based Brillouin laser and it can be suppressed by the use of a narrow band-pass filter in the laser configuration.

3.3 Experimental Methodology and Results

3.3.1 Laser Dynamics

Figure 3.5a illustrates a scheme of the experimental setup to study the emission dynamics of the random Brillouin fibre laser. In Figure 3.5a, a fibre laser with 3.5 kHz linewidth (Rock Module, NP Photonics) is amplified to 15 mW by a C-band erbium-doped fibre amplifier (EDFA) (FAF-50, INO) and launched into one end (in) of a 25 km single-mode BG fibre (SMF-28, Corning) via Port 2 of a fibre circulator (FCC1), acting as the pump light in SBS. The Stokes light out of the BG fibre is sent into a 10 km RSF fibre (SMF-28, Corning) via Port 2 of the FCC2, working as the pump light of Rayleigh scattering. The Rayleigh backscattered Stokes light accumulates along the RSF fibre and is then launched into the other end (out) of the BG fibre via Port 3 of the FCC2, working as the seed of consequent SBS amplification processes, while the forward Stokes light out of the RSF fibre through an isolator (ISO) acts as the laser output. A C-band narrow tunable filter (TFC, TeraXion) with 3-GHz bandwidth is used to remove the pump from the laser output. Analysis of the spectral and temporal output properties of the random Brillouin fibre laser are respectively completed by an optical spectrum analyzer (OSA) (AQ6370C, Yokogawa) and an oscilloscope (Scope) (WaveRunner 64Xi-A, Teledyne LeCroy) with a variable optical attenuator (VOA) and a photodetector (PD1) with 350-MHz bandwidth (PDB 130C-AC, Thorlabs). The fusion spliced fibre links between all the optical components ensure that no highly reflective surfaces dominate over the scattering light from the RSF fibre. Figure 3.5b

shows a typical spectrum analyzer display that the narrowband spectral output is constantly observed. Scope traces (10 MS/s) in Fig. 3.5c shows that occasional massive loss followed by non-periodic self-pulsing regimes eventually leads back to a quasi-DC component implying temporal fluctuations of the laser intensity. The usage of the AC-coupled PD1 indicates that the quasi-DC signals of the random Brillouin fibre laser output power fluctuates within a range of ~0.2 V as shown in Fig. 3.5c while another DC-coupled PD2 (PDB 130C-DC, Thorlabs) is used for intensity monitoring of the DC component, obtaining a value of ~0.95 V as shown in the inset of Fig. 3.5c. It corresponds to a power change by 21% that agrees well with the simulation result. In Fig. 3.5d-I, the quasi-DC signals (350 MS/s) with small time-series fluctuations present non-periodic chaotic behavior, and Scope traces of the PD1 dark-current noise is presented as well. Figure 3.5d-II shows that compared to that of the PD1 dark-current noise, the power spectrum of the random Brillouin fibre laser exhibits a distinct plateau occurring below around several tens of MHz due to significant mode-hopping/competition caused by the Rayleigh distributed feedback, confirming MHz-level bandwidth of the random Brillouin fibre laser. The inverse of its bandwidth, i.e. the chaotic oscillation duration of the highly unstable short-pulse trains in the quasi-DC component, in general is approaching to the phonon lifetime of silica τ_{phonon}. As shown in Fig. 3.5c, the occurrence of the large-scale self-pulses is unpredictable, while the duration of the quasi-DC signals could last for nearly hundreds of milliseconds that ensures a sufficient number of round-trip passes considering the sub-millisecond timeframe that light takes to travel around the cavity,

and consequently maximise the DMC in the practical power spectrum monitoring.

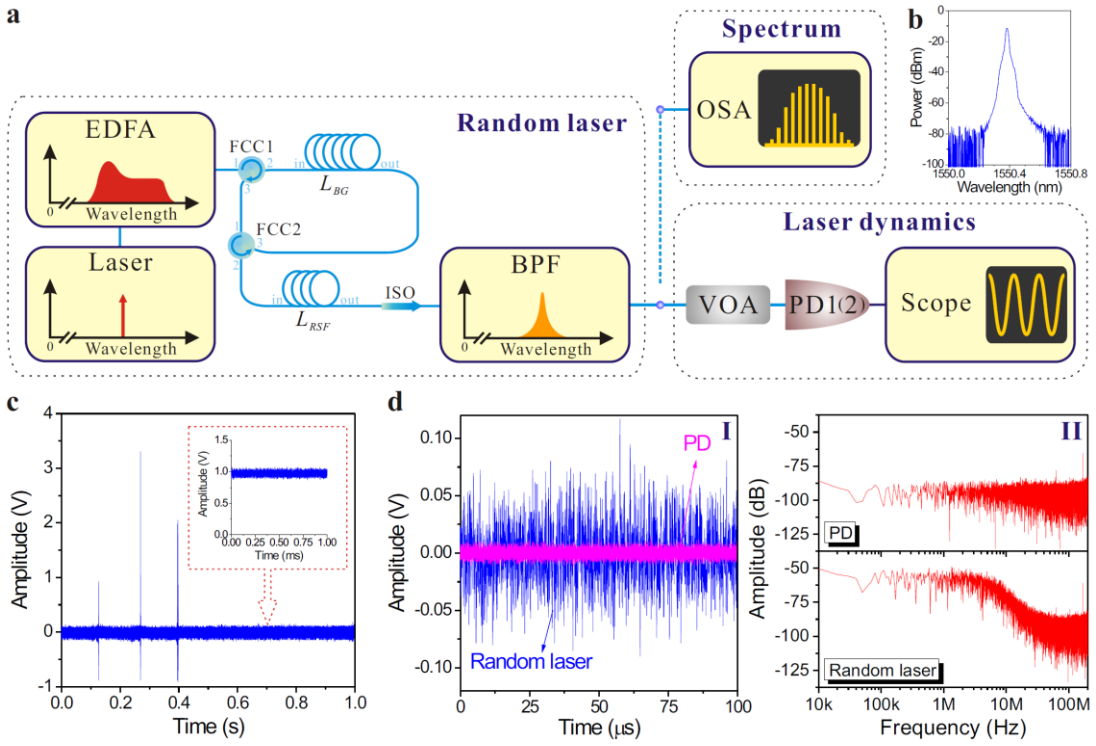

Figure 3.5 | **a,** Experimental setup of characterizing the random Brillouin fibre laser. **b,** A typical laser output spectrum. **c,** Time-series of the output fluctuations recorded on the Scope using the PD1, and inset is obtained using the PD2. **d,** (I) Temporal fluctuations of the random Brillouin fibre laser as well as the PD1 dark-current noise. (II) Power spectra of (top) PD1 dark-current noise and (bottom) random Brillouin fibre laser intensity fluctuations.

3.3.2 Microwave signal generation

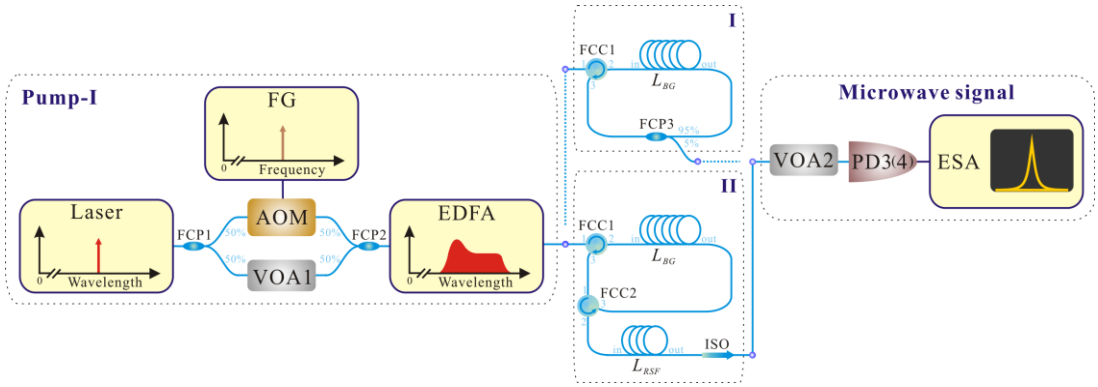

Figure 3.6 | Experimental setup of generating ultra-narrow linewidth microwave signals by the use of a fibre laser or a DFB laser and an AOM. (I) a gain medium, (II) a combined gain-feedback structure.

Figure 3.6 illustrates a scheme of the experimental setup to create an ultra-narrow beat signal from heterodyning two uncorrelated stimulated Brillouin Stokes waves by using a RSF fibre. In Fig. 3.6, the pump laser produces a light beam that is split into two arms through a 50/50 fibre coupler (FCP1). An acoustic-optical modulator (AOM) in one arm is controlled by a function generator (FG) to apply a specific frequency downshift to one light beam, and a VOA1 in the other arm is used to equalise the optical power of the two light beams. The two light beams are combined by a 50/50 FCP2 and amplified to 30 mW by the EDFA. Two Brillouin Stokes light beams from either a gain medium (I) or a combined gain/random-feedback structure (II) are mixed and the beat signal is analyzed by the microwave signal detection system equipped with a VOA2, a PD3 with 3-dB bandwidth of 3.5-GHz (1592, New Focus) and an electrical spectrum analyzer (ESA) (E4446A, Agilent). The VOA2 is utilised to adjust the output power and remove the Brillouin laser pedestal without influencing the microwave signal generation. The high sampling rate of the PD3 compared to the bandwidth of the random Brillouin fibre laser and the millisecond-level sweep time of the ESA compared to the temporal variation in phase over a relative short period confirms the validity of the microwave signal measurement.

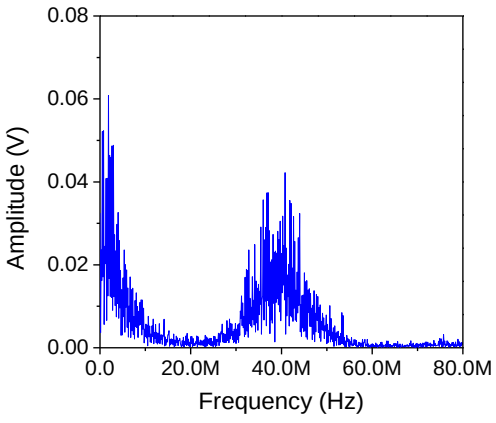

Figure 3.7 | Typical power spectra of the beat signals using the configuration of (Fig. 3.6-I) where the fibre laser is used.

In the ring structure (Fig. 3.6-I) sharing a common nonlinear gain medium for the two pump beams, the backscattered Stokes light from Port 3 of the FCC1 are sent back to Port 95% of a FCP3 and the other end (out) of the 25 km BG fibre to seed the SBS amplification process. By using the setup in Fig. 3.6-I, it only shows a noisy Brillouin gain spectrum in Figure 3.7, indicating that the generated Stokes waves from two Brillouin ring lasers, where a fibre laser (Rock Module, NP Photonics) works as the pump laser and an AOM is controlled by a function generator to apply a 40-MHz frequency downshift to one light beam, experience completely different SBS amplification processes, leading to very low degree of mutual coherence and asynchronous phase evolution.

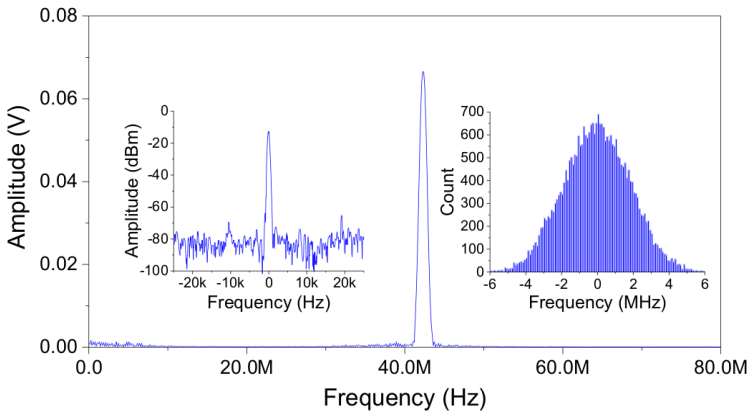

Figure 3.8 | Power spectra of the beat signals using the configuration of (Fig. 3.6-II) where the fibre laser is used. Insets are (left) the power spectrum in the 50-kHz span and (right) the coherent spike frequency jitter statistics. Zero frequency represents 40-MHz spectral spacing of the AOM.

When the two SBS Stokes light beams are launched into the same RSF fibre to ensure the same entropy source in the gain-feedback structure (Fig. 3.6-II) and the Rayleigh backscattered Stokes light is sent back to the BG fibre to ensure a

continuous flow of light, beat signals from the Stokes light beams out of the RSF fibre through the ISO are recorded to characterise the mutual coherence and spectral performance. Figure 3.8 (with Fig. 3.6-II) exhibits an obvious coherent spike in the power spectrum and the left inset of Fig. 3.8 shows an ultra-narrow coherent spike with 70-dB contrast in the 50-kHz span. The 20-dB spectral linewidth should actually be much smaller than ~1 kHz, since it corresponds to the Dirac delta function although limited by the resolution bandwidth of the ESA for a specific frequency scanning range. However, it is difficult to capture such coherent spikes because of frequency jitters of the coherent spike within a few MHz range in a 3-hour observation course as shown in the right inset of Fig. 3.8.

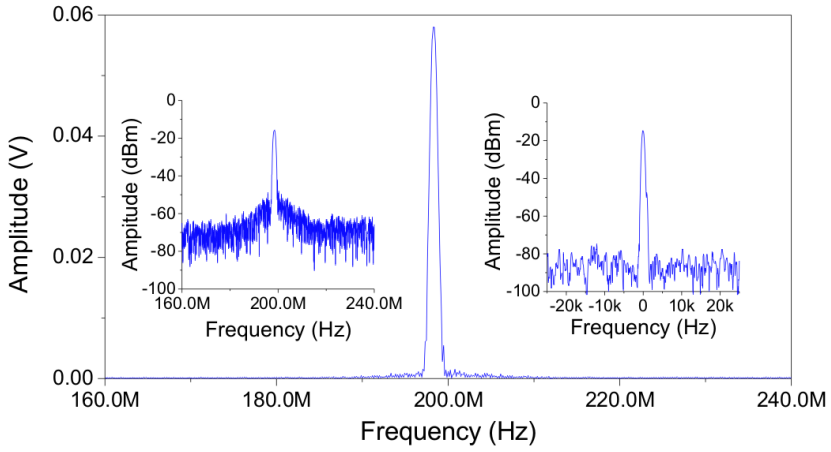

Figure 3.9 | Power spectrum of the microwave signal generated by the use of the DFB laser. Insets exhibit the power spectrum with a logarithmic amplitude axis in the 80-MHz span (left) and 50-kHz span (right). Zero frequency represents 200-MHz spectral spacing of the AOM.

Figure 3.9 shows another ultra-narrow microwave signal can be generated by using a distributed feedback (DFB) laser (CQF413/108, JDSU) of 2-MHz linewidth and an AOM with a spectral spacing of 200 MHz. In the left inset of Figure 3.9, the same power spectrum with a logarithmic amplitude axis distinctly displays a random

Brillouin laser pedestal with MHz-level bandwidth besides an ultra-narrow coherent spike with ~40-dB contrast due to the low resolution of the ESA in the 80-MHz span, while the contrast resumes ~70-dB as the 50-kHz span is adopted as shown in the right inset of Figure 3.9.

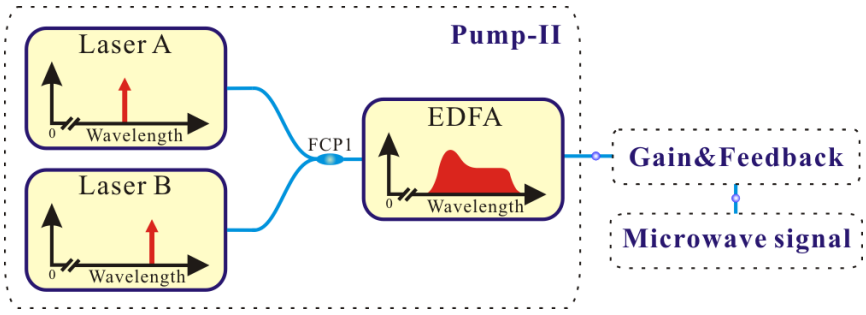

Figure 3.10 | Experimental setup of generating ultra-narrow linewidth microwave signals by the use of two separate lasers.

The ultra-narrow microwave signals at any given frequency can in principle be produced by any two completely independent pump lasers without any extraordinary demands of pump sources to be narrow linewidth and expensive external optical modulators, as shown in Fig. 3.10. Figure 3.11a demonstrates the microwave output with a tuning range up to 23 GHz by using two separate fibre lasers. In Figure 3.11a, a much larger frequency difference between two laser beams cannot be detected since it is restricted by the 25-GHz bandwidth of the PD4 (1414, New Focus). Furthermore, the super-narrow microwave signal generation can even be achieved using an external cavity laser (Planex, RIO) and a compact tunable laser (81980A, Agilent), as shown in Figure 3.11b. All these coherent spikes consistently remain at an ultra-narrow level of linewidth.

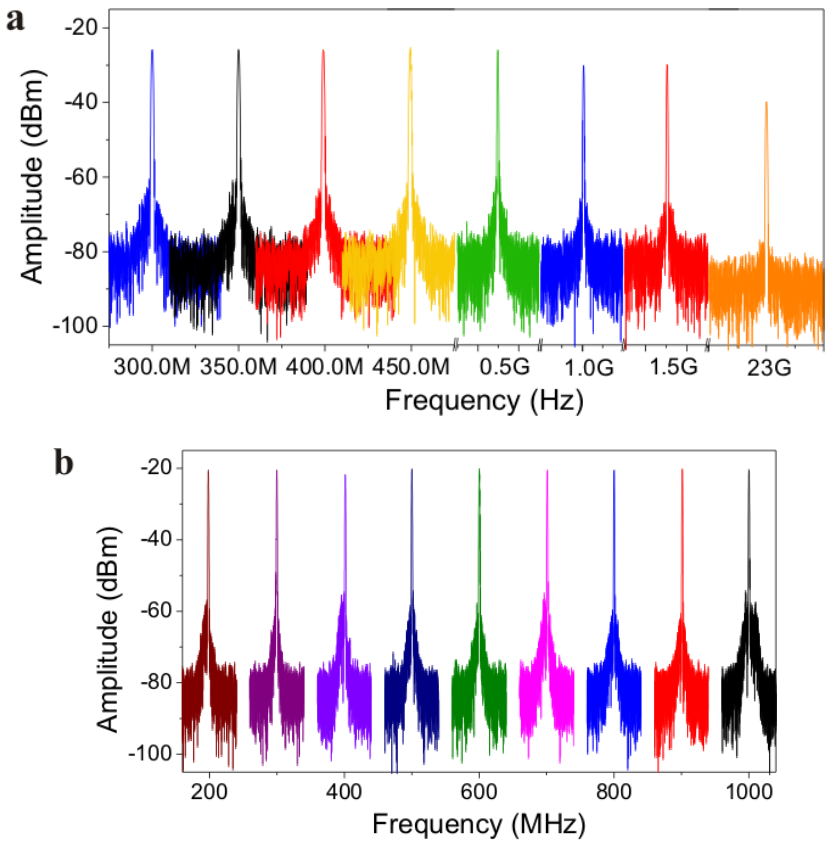

Figure 3.11 | **a,** Typical power spectra of the tunable microwave signals generated by two same lasers. **b,** Typical power spectra of the tunable microwave signals generated by two different lasers.

3.4 Conclusions

We have successfully proved that the generation of high-purity RF signals can be achieved by using the ultra-long standard telecommunication optical fibres only, without any extraordinary demands of the pump source with narrow line-width and the expensive external optical modulator. In addition, our scheme would readily generate a signal with higher beat-tone frequency up to the terahertz (THz) range by using a high-bandwidth photomixer, where the frequency drift of a few megahertz can be reasonably ignored. This novel approach has a great potential in creating millimeter-wave and THz frequencies that remain one of the most underdeveloped

frequency ranges. The proposed scheme is promising for various applications in remote sensing, spectroscopy, and communications. For instance, the THz radiation can be produced for wireless communication and photonic local oscillators [40], its high sensitivity to environmental perturbation can be used in phase-sensitive time-domain reflectometry based on Rayleigh scattering [41], the intrinsic random properties of the microwave signals might be employed in random bit generation [42] and secret key exchange for laser cryptography [43].

Chapter 4

Random Fabry-Pérot resonator-based sub-kHz Brillouin fibre laser to improve spectral resolution in linewidth measurement

4.1 Introduction

Laser linewidth characterization has been extensively studied when narrow-linewidth lasers are massively employed in many fields such as telecommunications, atomic physics, microwave generations and metrology [44-46]. As one of the most important parameters of lasers, laser spectra are commonly regarded as a benchmark for the laser performance. Conventional diffraction grating based or Fabry-Pérot interferometer based optical spectrum analyzers [47, 48] have suffered from strong limitations in high-resolution and high-dynamic-range measurements. Other techniques transforming phase fluctuations to intensity variations by optical heterodyne or homodyne detections using two-path optical circuits like Mach-Zehnder and Michelson interferometers [49, 50] have realised high resolution up to kilohertz. However, prerequisite conditions such as uncorrelation between the signal and a replica of itself with a modulated frequency must be met in order to obtain a precise beating signal without any contributions from coherence. Technical difficulties emerge especially for the linewidth interpretation of narrower lasers where a very long delay line is needed. To

overcome the drawbacks of high loss and technical problems brought by extremely long fibre delay line, the loss-compensated recirculating delayed self-heterodyne interferometer (LC-RDSHI) [51, 52] whose delay line is not required to be longer than the coherent length of laser under test was developed for narrow linewidth measurement. But the resultant beating signals are inevitably degraded by the multi-interferences due to the recirculation and then complicated signal processing methods must be adopted to remove the negative effects.

The spectrum analysis was also assisted by the SBS effect, for example, characterizing either the amplified Stokes light or the beat tone heterodyning the amplified narrow Stoke light and the signal under test [53, 54]. They have been reported to achieve a high frequency resolution up to 10 MHz limited by the Brillouin gain bandwidth over the whole C and L telecommunication bands. However, additional scanning tunable laser is needed to reconstruct the spectrum of signal under test. Another novel method based on the Brillouin fibre laser (BFL) was later proposed to get rid of the extra optical source [55], which only utilises the laser under test itself. The spectrum of beating signal by heterodyning the build-up BFL and part of the light from laser under test was analyzed with a finer resolution up to kHz which is restricted by the properties of the constructed BFL. The main drawback of possible multi-mode lasing, however, deteriorates the stability of the BFL.

In this chapter, we propose, for the first time, a novel Brillouin random fibre laser based on bi-directional pumping scheme, which has achieved a lasing output with narrow linewidth of ~860 Hz. A new model of random fibre Fabry-Pérot resonator which is built up through the pump depletion effects of stimulated Brillouin scattering and the feedback of Rayleigh backscattering is developed to understand the physics behind the bi-directionally pumped

Brillouin random fibre laser. Compared with traditional linewidth characterization based on the delayed self-heterodyne technique, where a 200-km fibre must be used in order to achieve 1-kHz resolution of the linewidth measurement, the proposed extremely simple and compact narrow-linewidth laser provides a new tool for narrow linewidth characterization of less than 1 kHz by using only a 10-km fibre.

4.2 Theory Model

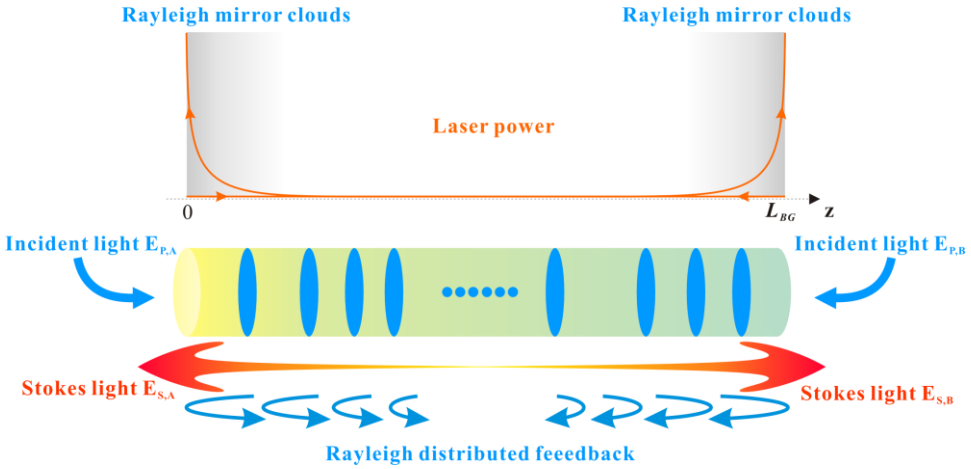

Figure 4.1 | Configuration of random fibre FP resonator based Brillouin fibre laser.

The configuration of the random fibre Fabry-Pérot (FP) resonator is shown in figure 4.1. As optical beams $E_{P,A}$ and $E_{P,B}$ with equal power from the same source are launched into the two ends of the optical fibre respectively, they would be scattered from the refractive index fluctuation associated with an acoustic pressure wave of frequency Ω_B, leading to the generation of Brillouin Stokes light that propagates opposite to the pump light and has a frequency downshift of Ω_B with respect to the pump light due to the Doppler effect. The Stokes light $E_{S,A}$ (or $E_{S,B}$) is amplified through the nonlinear electrostriction mechanism along the Brillouin gain fibre. Once pump depletion is triggered as the gain parameter $G=gI_P(0)L$ is well above the threshold for SBS, the effective amplification length is not the length of optical

fibre L but determined by $I_s(L_{eff})=I_s(0)/e$. As a consequence, most energy of Brillouin Stokes light is stored in both ends of the gain fibre. It is noticed that higher-order Stokes light generation in cascaded SBS process is significantly suppressed because of the short interaction length between the first-order Stokes light and the acoustic pressure wave. Another co-existing scattering mechanism is the Rayleigh scattering which provides the random phase feedback, forming the distributed Rayleigh mirrors. However, only the Rayleigh mirrors located within the pump depletion regions where stores the majority of SBS Stokes light energy are capable of offering effective feedback and form two "mirror clouds" at both ends of the fibre, as shown in figure 4.1. Although the reflection coefficient of the distributed Rayleigh mirrors is extremely small (~7.3×10^{-5}/km), the SBS amplification induced by another pump source is great enough to compensate for this loss. Consequently, the two Rayleigh mirror clouds located at both ends of the optical fibre constitute the random Fabry-Pérot resonator.

Note that the cavity length L_{Ray} is not constant for the random fibre FP resonator and follows a random process statistically with the expected value L_0 which is approximately equal to $2L$ and the standard deviation σ_L. Therefore, non-periodic interference patterns in the spectra are expected due to a random distribution of the optical path length for an arbitrary round-trip, leading to lasing for some spectral components inside the SBS gain profile. If the polarization effect is omitted, the optical field emitted from the output port A is given by

$$E_{out,A}=\sum_{k=1}^{N}E_{S,A}\prod_{m=1}^{k}e^{-\alpha L_{Ray,m}}G_{A,m}R_{2m}G_{B,m}R_{2m-1}e^{-i2\pi\frac{\nu}{c}nL_{Ray,m}} \tag{4.1}$$

where $L_{Ray,m}$ is the optical path length of m-th round-trip; α and n are the mean loss coefficient and refractive index respectively; $G_{A,m}$ and $G_{B,m}$ are the SBS amplification coefficients for m-th round-trip induced by pump light $E_{P,A}$ and $E_{P,B}$ respectively; R_{2m-1} and R_{2m} are the distributed Rayleigh reflection coefficients in energy-stored regions near port A and port B respectively; v is the optical frequency and c is the photon velocity in vacuum.

The Power evolutions of the pump light $P_{P,A}$ and $P_{P,B}$, SBS Stokes light $P_{S,A}$ and $P_{S,B}$ in the gain fibre are given by

$$\begin{cases} \dfrac{\partial P_{P,A}}{\partial z} = -g_B P_{P,A}(P_{S,A} + rP_{S,B} + 2\sqrt{rP_{S,A}P_{S,B}}) - \alpha P_{P,A} + rP_{P,B} \\ \dfrac{\partial P_{S,A}}{\partial z} = -g_B P_{S,A}(P_{P,A} + rP_{P,B} + 2\sqrt{rP_{P,A}P_{P,B}}) + \alpha P_{S,A} \\ \dfrac{\partial P_{P,B}}{\partial z} = g_B P_{P,B}(P_{S,B} + rP_{S,A} + 2\sqrt{rP_{S,A}P_{S,B}}) + \alpha P_{P,B} - rP_{P,A} \\ \dfrac{\partial P_{S,B}}{\partial z} = g_B P_{S,B}(P_{P,B} + rP_{P,A} + 2\sqrt{rP_{P,A}P_{P,B}}) - \alpha P_{S,B} \end{cases} \tag{4.2}$$

where g_B is the Brillouin gain factor; α is the linear loss coefficient and r is the Rayleigh backscattered coefficient.

Table 4.1. Simulation parameters

SBS gain fibre	
Fibre type	SMF-28
L (km)	10
g_B ($m^{-1}W^{-1}$)	0.21
α (m^{-1})	$4.4\cdot10^{-5}$
r (m^{-1})	$7.3\cdot10^{-8}$
$P_{P,A}\|_{z=0}$, $P_{P,B}\|_{z=L}$ (W)	0.035
$P_{S,A}\|_{z=L}$, $P_{S,B}\|_{z=0}$ (W)	$0.66\cdot10^{-9}$

Using Eq. (4.2) and simulation parameters listed in Table 4.1, the power distributions of $P_{P,A}$, $P_{P,B}$, $P_{S,A}$ and $P_{S,B}$ along the SBS gain fibre were simulated. As shown in figure 4.2, P_S experiences an exponential growth only in a relatively short length at both ends of the fibre,

accompanying with strong depletion effects of P_P. The effective amplification length is calculated around 0.25 km which offers estimations for $L_0 \approx 19.5$ km and $\sigma_L \approx 0.5$ km.

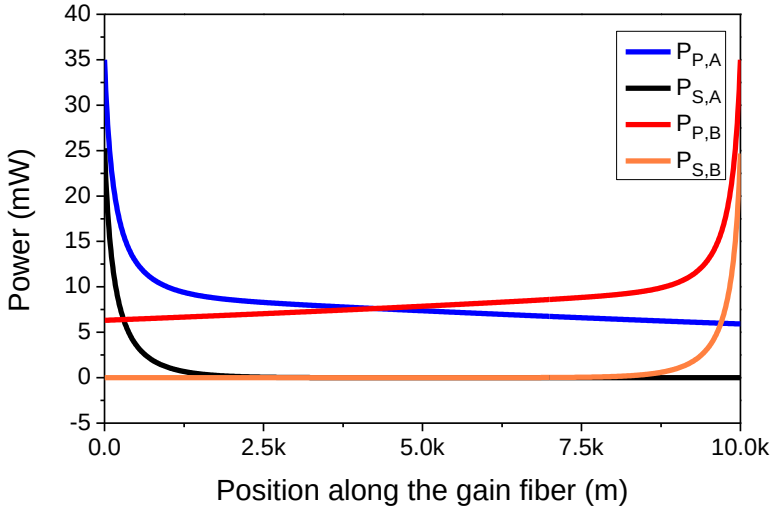

Figure 4.2 | Power evolutions of pump and Stokes lights in SBS gain fibre.

Figure 4.3a reveals the random resonance feature of the random FP resonator. The numerically simulated spectrum is a result of a coherent superposition of multiple round trips with complex photon trajectories by using Eq. (4.1), which exhibits a chaotic interference pattern and the resonance spike appearing at stochastic positions. If an unflattened SBS gain profile is adopted, the resonant lasing spikes would preferably occur in the frequency region where the Brillouin gain could overcome the total cavity loss, leading to the generation of random lasing behavior. Note that the condition that σ_L is much less than L_0 is automatically satisfied in this kind of random fibre laser and plays a pivotal role in such narrow-band lasing emission. The simulated statistical distribution of frequency jitters is shown in figure 4.3b. It obtains the opportunity of narrow radiation but at the cost of frequency stability.

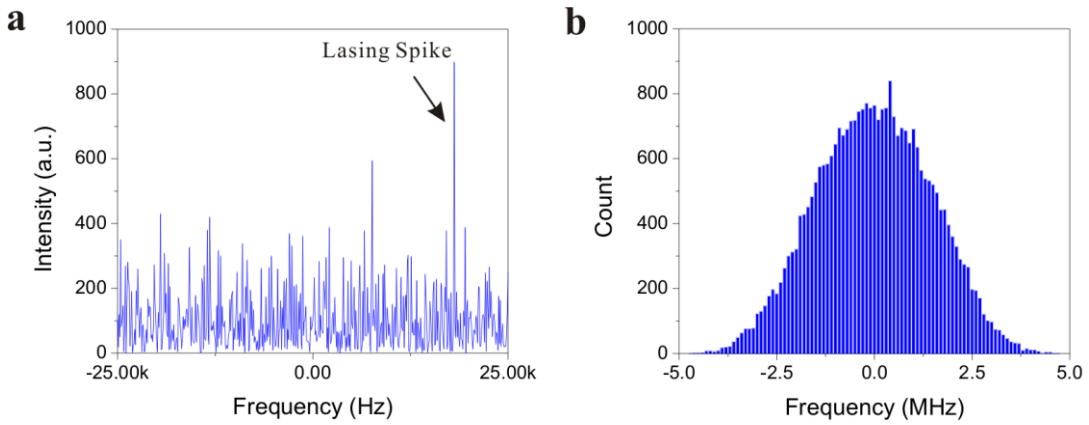

Figure 4.3 | Numerical simulation results. **a,** Non-periodic interference pattern in optical spectra of random FP resonator. **b,** Statistical distribution of the lasing frequency jitters in a 10-MHz span.

4.3 Experimental Methodology and Results

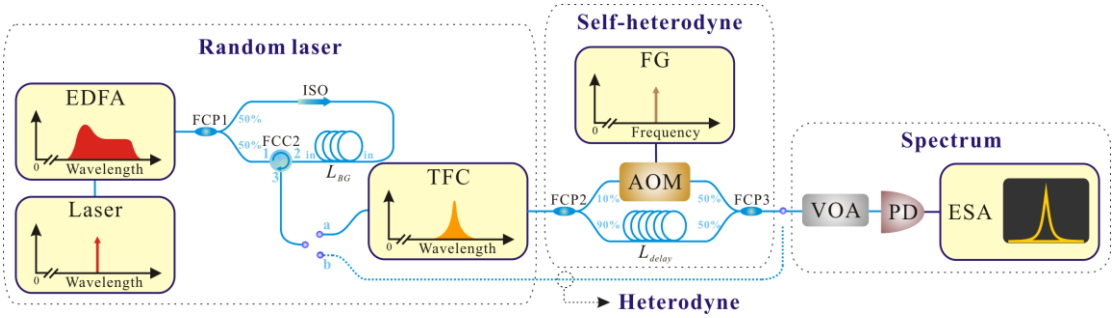

Figure 4.4 | Experimental setup of the random fibre FP resonator based Brillouin fibre laser. 3→a: Conventional delayed self-heterodyne method; 3→b: Proposed linewidth measurement method.

The experimental setup of the random Brillouin fibre laser is shown in the upper part of figure 4.4. Light from a fibre laser (Rock Module, NP Photonics) with a linewidth of ~3 kHz is amplified by an EDFA (APEDFA-C-10-B-FA, Amonics) and then split into two equal parts by a 50/50 coupler (FCP). The bi-direction pumping scheme is built up by launching each part of lights to each end of a 10-km-long single mode fibre (SMF-28, Corning) inside an aluminous soundproof box isolating from external disturbance. An isolator is inserted in the upper light path to protect the EDFA from the backward scattered Stokes light. To guarantee a highly pure Stokes lasing output, a narrow optical filter (TFC, TeraXion) with 3-GHz

bandwidth is used to remove the un-depleted pump light from the output at port 3 of the circulator (FCC). The threshold power of the proposed laser was measured to be 10mW for each pump light by varying the amplification magnitude of the EDFA as shown in figure 4.5a.

It is necessary to characterise the linewidth of the proposed random Brillouin fibre laser (RBFL) itself before being applied in linewidth measurement for other light sources. A conventional delayed self-heterodyne (DSH) method is employed by connecting port 3 of the circulator with port (a) in figure 4.4. The laser output is divided into two arms by a 90/10 coupler. An acoustic-optical modulator (AOM) in one arm is controlled by a function generator (FG) to apply a specific frequency downshift to one light beam, and the 250-km SMF in the other arm is used as optical delay line. The two light beams are mixed by a 50/50 FCP and the beat signal is analyzed by the microwave signal detection system equipped with a photodetector with 350-MHz bandwidth (PDB 130C-AC, Thorlabs) and an electrical spectrum analyzer (ESA) (E4446A, Agilent). The experimental result is given in figure 4.5b, which shows a -20dB linewidth of ~17.2 kHz corresponding to 860.0 Hz for -3dB linewidth. The resultant linewidth arises from the narrowing effects induced by the random fibre FP resonator that is built up on bi-direction pumped SBS processes at both ends of the 10-km optical fibre. Although the lasing threshold is dependent largely on the pump-Stokes interaction length as well as the coherent Rayleigh feedback, the optical fibre length has little influence on the linewidth of the proposed random laser once the lasing is initiated. Based on aforementioned facts, the proposed RBFL could be utilised as an effective reference for measuring linewidth beyond 860 Hz.

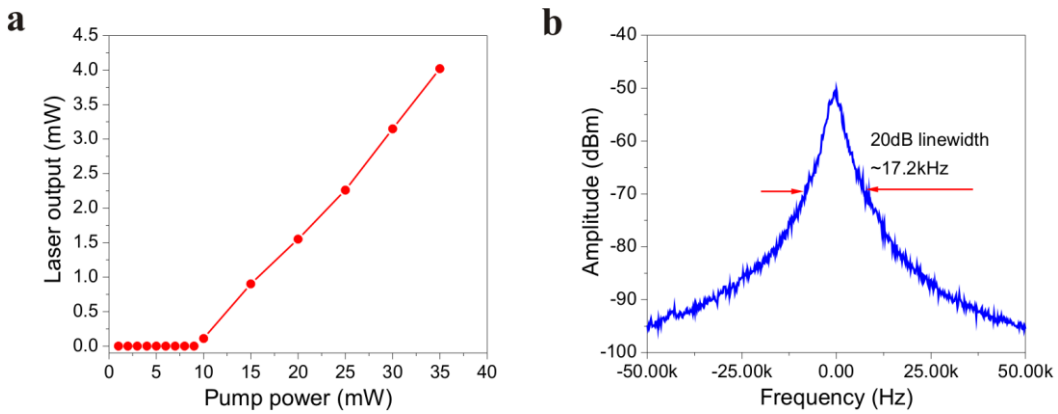

Figure 4.5 | **a,** Measured output powers as the function of pump powers. **b,** Linewidth of the proposed RBFL measured by self-heterodyne method.

Characterizing the linewidth of the pump laser is carried out by connecting port 3 of the circulator with port (b) in figure 4.4. The detected signal is the power spectrum of the beat signal between the pump light and Stoke lasing light centered at 10.87 GHz. Their optical powers are equalised approximately in order to obtain the optimal visibility. Due to the unique feature of the random FP resonator induced by pump depletion effect of SBS, the beat signal drifts within a range of several Megahertz, which could be attributed to the following two reasons. Firstly, the random FP resonator is built up on pump depletion at both ends of the 10-km Brillouin gain fibre embedded by mirror clouds with 250m long within which Rayleigh mirrors are randomly distributed and the Rayleigh scattering of the Stokes light dominates compared with other regions of the fibre. The phase shift term $2\pi m\nu L_{Ray,m}/c$ in Eq. (4.1) induced by any two Rayleigh mirrors located at each end of the fibre varies with time, leading to an intermittent change of the resonant frequency. In addition, the thermally fluctuating refractive index of optical fibre would force the Brillouin gain profile to drift slowly from its original center resulting in the occurrence of coherent resonance at different frequency within drifting range. The thermal drift is estimated within a 2-MHz range given that the temperature fluctuation is normally ±1°C in the lab environment [56]. Frequency jitter

statistical experiment is performed by collecting 30000 spectra within a time period of three hour as shown in Fig. 4.6.

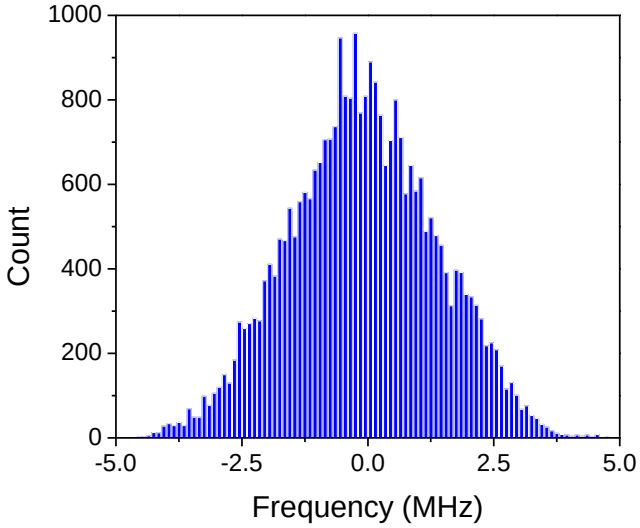

Figure 4. 6 | Experimental statistical distribution of the lasing frequency jitters in a 10-MHz span.

The linewidth measurement was carried out by capturing the beat spectra from ESA within a frequency span of 1 MHz centered at 10.87 GHz. Following the statistical result from figure 4.6, the probability of the beat signal showing up within the specified span is estimated to be ~17.3%, which agrees well with the practical operation that one out of 5 or 6 times of single measurements would capture one beat signal. The measurement result is given in figure 4.7a where the linewidth profile is acquired by averaging over 20 spectra to remove undesired noises. To demonstrate the validity and accuracy of this proposed method, another linewidth measurement obtained from the conventional DSH method with the use of 100-km optical delay line is exhibited in figure 4.7b for comparison. The linewidth of the NP fibre laser is measured to be 2.835 kHz, which agrees well with that acquired from conventional DSH method with a value of 3.00 kHz.

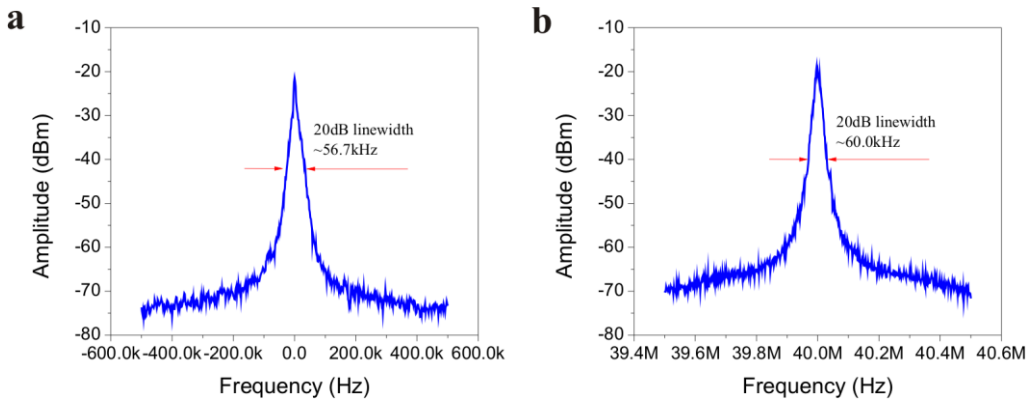

Figure 4.7 | **a,** Laser linewidth measurements via proposed method. **b,** Laser linewidth measurements by using conventional DSH method.

4.4 Conclusions

In summary, a novel Brillouin random fibre laser is theoretically and experimentally proposed and demonstrated. The random fibre FP resonator is built up through pump depletion effects of SBS based on the unique bi-direction pumping scheme. A novel theoretical model is developed to elaborate the operation mechanism of the proposed random laser. Experimental results show that the proposed laser emits radiation with a narrow linewidth of ~860 Hz and could be effectively utilised to characterise the linewidth at accuracy of less than 0.9 kHz.

Chapter 5

Physical Random Bit Generation with Random Brillouin Fibre Laser

In last chapter, we have proposed and experimentally demonstrated a new type of a random laser operating via random distributed scattering in the standard optical fibre. In the present chapter, we will see the random distributed feedback laser practically radiates the spatially confined light in quasi-CW regime. The physical origin of chaotic behavior of laser output will be studied and also its application in fast random number generation will be explored.

5.1 Introduction

Random bit generators (RBGs) are crucial in cryptography, secure communications [57], Monte-Carlo simulation [58], and stochastic modelling [59]. The methods used for RBG can be divided into either software-based or physical-based approaches [60]. Deterministic algorithms are easily implemented in any computational platform to generate pseudo-random numbers and they are only limited by the processor speed. However, it is not truly random because the same initial state can produce identical sequences. So it is vulnerable, especially when partial knowledge about the algorithm or its initial state is disclosed.

Truly random bits generation must rely on intrinsically non-deterministic physical

processes. For example, a variety of unpredictable phenomena such as thermal noise in resistors and photon noise have been used as physical entropy sources for non-deterministic generators [61, 62]. In 2008, Uchida and colleagues [63] have demonstrated a 1.7 Gbit/s generator based on the binary digitization of two independent chaotic semiconductor lasers. After that, many works based on other random processes were triggered including amplified spontaneous noise [64], phase noise [65]. However, the properties of random Brillouin fibre lasers have never been studied towards this application.

In this chapter, the fluctuating intensity of a chaotic random Brillouin fibre laser (RBFL) is used for generating random sequences at rates up to 7.1 Mbps. The generator's simplicity and robustness enable its application to tasks of secure communication and calculation procedures requiring the generation of random bit sequences.

5.2 Operation Principle

Ideal phase-locked lasers are coherent light sources and radiate perfectly sinusoidal light waves over seconds. It starts from the initial noise that is spontaneously emitted with random phases and directions by atoms of gain medium without any incident seed photons. In addition, initial photons bounce back and forth between cavity reflectors and are colour-selectively amplified by stimulated emission. Such fixed cavity brings the fixed phase-matching condition and creates first-order coherence which is a measure of fluctuations of the field without considering the thermal

instability. Meanwhile, the definite number of gain atoms leads to the gain saturation effect so that the intensity simply cannot grow further and hence the intensity fluctuations are suppressed, leading to second-order coherence [66].

In the random lasing regimes, the situation changes dramatically. The resonant feedback in the bi-directional pumped random fibre laser is achieved by the refractive index irregularities distributed along the standard optical fibre but the effective Rayleigh mirrors are only localised in both fibre ends because of the pump depletion effect. Physically this means that the lucky photons captured in this open cavity follow complex yet a little constrained trajectories, conducting a localised random walk in the round-trip phase shift of the optical wavelets and then a unique interference effect. The build-up of radiation in this random laser benefits from the significant round-trips amplification supported by the designated dual-pumping approach, leading to the ultra-narrowband random-lasing envelope with an 860-Hz linewidth at the cost of frequency stability and intensity noise. The resonant lasing components appear at stochastic positions and keep continuously tuning inside the SBS gain owing to the random interference effect and the thermally induced fluctuation in Rayleigh scattering. The amplitudes of spectral components located in the SBS gain profile, thus, cannot be maintained the fixed values and the emission spectrum keeps continuously reshaping, leading to the chaotic intensity fluctuations in random fibre laser output. So, RBFL actually works as a partially coherent continuous-wave laser.

Numerical simulation of the SBS in this RBFL configuration was also performed.

A set of equations for complex amplitudes of the pump wave $A_P^{\pm}(z, t)$, the Stokes wave $A_S^{\pm}(z, t)$, and the hypersound wave $\rho^{\pm}(z, t)$ were used in the simulation:

$$\pm\frac{\partial A_P^{\pm}}{\partial z}+\frac{n}{c}\frac{\partial A_P^{\pm}}{\partial t}=i\kappa_1 A_S^{\mp}\rho^{\pm}-\frac{\alpha}{2}A_P^{\pm} \tag{5.1}$$

$$\pm\frac{\partial A_S^{\pm}}{\partial z}+\frac{n}{c}\frac{\partial A_S^{\pm}}{\partial t}=i\kappa_1 A_P^{\mp}\rho^{\mp *}+\eta^{\mp}A_S^{\mp}-\frac{\alpha}{2}A_S^{\pm} \tag{5.2}$$

$$\frac{\partial \rho^{\pm}}{\partial t}+\frac{1}{2}\Gamma_B\rho^{\pm}=i\kappa_2 A_P^{\pm}A_S^{\mp *}+f^{\pm} \tag{5.3}$$

being

$$\kappa_1=\frac{\gamma_e\omega_P}{4nc\rho_0} \text{ and } \kappa_2=\frac{\gamma_e\omega_P}{c^2\upsilon A_{eff}}$$

where n is the mean refractive index of the core and c is the light speed in vacuum; α is the linear loss coefficient; κ_1 and κ_2 are Brillouin coupling constants; υ and Γ_B are the sound velocity and the phonon decay rate, respectively; γ_e and ρ_0 are the electrostrictive constant and density of silica, respectively; ω_p is the pump wave frequency and A_{eff} is the effective mode area; ± denotes counter-propagating waves. Rayleigh backscattering coefficients $\eta^{\pm}(z)$ and the Langevin noise source $f^{\pm}(z, t)$ follow the Gaussian random processes with zero mean: $\langle\eta^{\pm}(z')\ \eta^{\pm *}(z'')\rangle=r\delta(z'-z'')$, where r is Rayleigh reflection coefficient; $\langle f^{\pm}(z', t')\ \eta^{\pm *}(z'', t'')\rangle=Q\delta(z'-z'')\delta(t'-t'')$, and Q is noise intensity [9]:

$$Q=\frac{2k_BT\rho_0\Gamma_B}{\upsilon^2 A_{eff}} \tag{5.4}$$

where k_B is the Boltzmann constant, and T is the environmental temperature. The values of all coefficients used in simulation are: n=1.45, c=3×10^8 m/s, α=4.4×10^{-5} m^{-1} υ=5.96×10^3 m/s, Γ_B=1/τ_{phonon}=0.1 GHz, γ_e=0.902, ρ_0=2210 kg/m^3, ω_p=1.22×10^{15} rad/s, A_{eff}=50 μm^2, r=7.3×10^{-8} m^{-1}, k_B=1.381×10^{-23} J/K, T=300 K, and the fibre length L_{BG}=10 km.

The simulated result of the laser dynamics is shown in the inset of figure 5.1. The optical Stokes wavelets with dynamic phase shifts are scattered from fluctuations of thermodynamic quantities, proceeding to the SBS process in counter-propagating direction. The power spectral density (PSD) of the thermal noise throughout its frequency spectrum is restrained by the finite bandwidth of the SBS gain, so the chaotic oscillation period of the Stokes power could be very short approaching to τ_{phonon}. Thus, this system exhibits the chaotic behavior in the form of fast random-intensity spikes with random amplitudes and time positions, which means that the probability that a next value in the time series will be over or below the mean value is independent of both the recent history and the current amplitude. This is indeed the property of chaotic trajectories along which the laser intensity fluctuates. Therefore, the chaotic systems are good candidates for fast and simple physical entropy sources and generate efficient and stable random bits at relatively high frequencies.

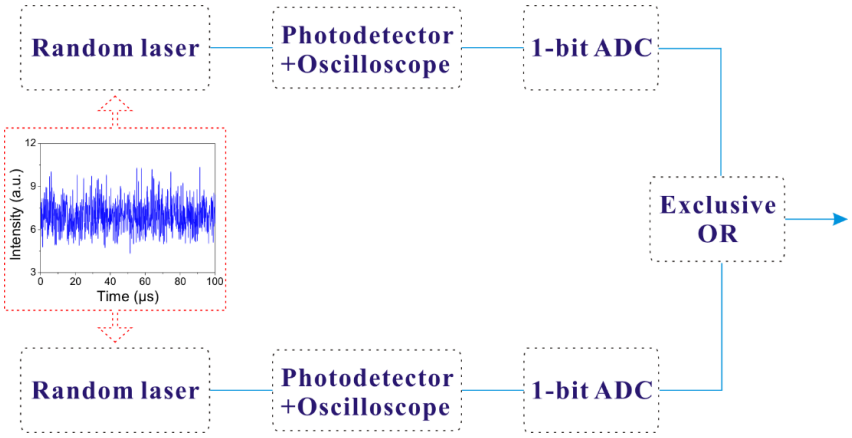

Figure 5.1 | Schematic diagram. Inset is the simulated chaotic intensity fluctuations of the random fibre laser output.

The scheme for generating random bit sequences is shown in figure 5.1. The chaotic intensity oscillations are provided by two inherent and independent laser

outputs from the random fibre Fabry-Pérot (FP) resonator. Each output intensity is converted to an a.c. electrical signal by photodetectors and converted to a binary signal using a 1-bit analog-to-digital conversion (ADC) by sampling the electrical signal at each interval τ_s and comparing with a threshold. The non-deterministic property of the temporal waveforms from arbitrary laser output port is assured by individual chaotic dynamics. Additionally, combining the sequences from two RBFL output ports with incommensurate chaos can produce better quality random sequences. So, the binary bit signals obtained from the two laser outputs are combined by a logical exclusive-OR (XOR) operation to generate a single random bit sequence, leading to the completely unpredictability.

5.3 Experimental Methodology and Results

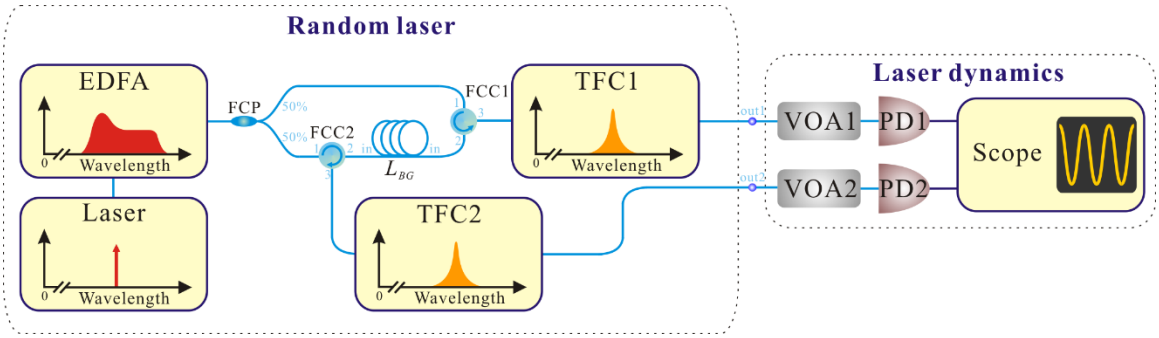

Figure 5.2 | Experimental setup of random bit sequence generator using RBFL.

A schematic of the experimental apparatus is shown in figure 5.2. A fibre laser with 3.5 kHz linewidth (Rock Module, NP Photonics) is amplified to 70 mW by a C-band EDFA (APEDFA-C-10-B-FA, Amonics) and then split into two equal parts by a 50/50 coupler (FCP). The bi-directional pumping scheme is built up by launching each part of lights to each end (in) of a 10-km single mode BG fibre (SMF-28, Corning) inside

an aluminous soundproof box isolating from external disturbance via Port 2 of fibre circulators (FCC1,2). Two C-band narrow tunable filters (TFC, TeraXion) with 3-GHz bandwidth are used to remove the pump from two laser outputs (out1,2), respectively. Analysis of the temporal output properties of the random Brillouin fibre laser is completed by an oscilloscope (Scope) (WaveRunner 64Xi-A, Teledyne LeCroy) with a variable optical attenuator (VOA) and photodetectors (PD1,2) with 3.5-GHz bandwidth (1592, New Focus).

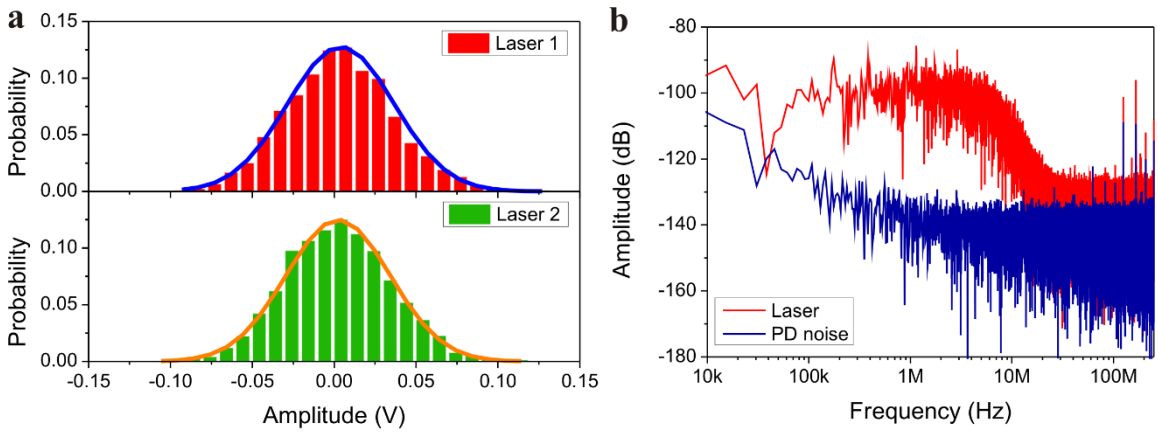

Figure 5.3 | **a,** Experimental histograms of the amplitude statistical distributions of two a.c. electrical signals and the Gaussian fit of corresponding experimental histogram. **b,** Power spectra of random Brillouin fibre laser power fluctuations and PD dark-current noise.

Figure 5.3a demonstrates that histograms of the statistical distributions of the RBFL output power calculated from the 100-μs digitised Scope traces (500 MS/s) correspond to the Gaussian law, which reveals that the generated random Boolean sequences via sampling these traces will be statistically unbiased (equal subsequent probability of 0 and 1). Having such unbiased distribution is a necessary but insufficient condition for a true random number generators. Figure 5.3b shows that compared to that of the PD dark-current noise, the power spectrum of the random

Brillouin fibre laser exhibits a distinct plateau occurring below around several tens of MHz due to significant mode-hopping caused by the Rayleigh distributed feedback. The bandwidth limits the chaotic oscillation rate of the highly unstable short-pulse trains in the quasi-DC output. Power autocorrelation function (ACF) also provides exact information about statistical properties of the generated random-lasing radiation and its definition is given by

$$C(\tau) = \frac{\langle P(t)P(t+\tau)\rangle}{\langle P(t)^2\rangle} \tag{5.5}$$

In figure 5.4, the correlation peaks decay rapidly over a few periods due to the strongly chaotic dynamics. The correlation time of approximately 0.14 μs sets the minimum sampling time interval τ_s, confined by the chaos bandwidth which is closely associated with the SBS characteristics.

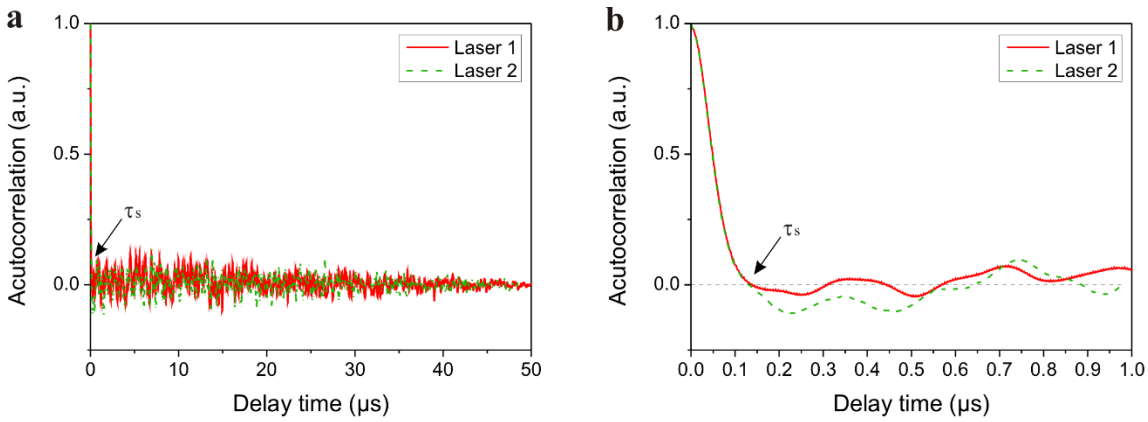

Figure 5.4 | Autocorrelation characteristics. **a,** Autocorrelation functions of the chaotic waveforms of two random-laser signals. τ_s, sampling time interval. **b,** Enlargement of the short-time autocorrelation.

Finally, an example of random bit generation at an achievable maximum rate of 7.1 Mbps, corresponding to the correlation time of 0.14 μs, with random fibre FP laser is realised. The temporal waveforms of the two chaotic outputs from RBFL, and the corresponding sequence of random bits output from the XOR operation are shown in

figure 5.5.

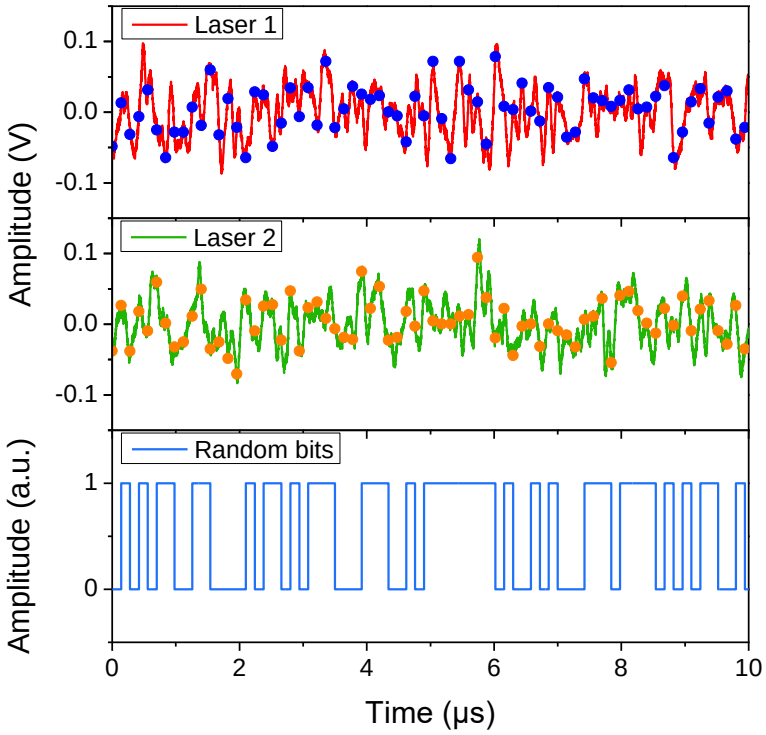

Figure 5.5 | Typical output signals from an experimental system: temporal waveforms of the laser output signals and the corresponding random bit sequence. Solid dots mark sampling points.

5.4 Conclusions

We have demonstrated that continuous streams of random bit sequences are generated at fast rates of up to 7.1 Mbps by directly sampling the two outputs of RBFL. The generator is simple to be implemented and has absolutely no requirements on either the timing of the digitization or on the average value of the laser output power. This system holds a large potential for improvements in performance of random number generators.

Chapter 6

Conclusions and Outlook

We have characterised the lasing properties of the novel random fibre ring laser and demonstrated theoretically and experimentally that the accumulated random phase over the ultra-long standard fibre can enhance the degree of mutual coherence between two Stokes signals, leading to a beat signal with a Dirac delta function profile in frequency domain. This allows us to synthesise high spectral purity microwave signals from Brillouin fibre lasers with randomised feedback. The proposed microwave sources will play a pivotal role in a multitude of applications in the information and communication technology, such as high-speed data processing, wireless telecommunications, phased-array radars, and remote distributed antenna systems. For example, the all-optical system allows extensions to fibre optical communication achieving data rates exceeding a terabyte per second.

We have also developed a random Fabry-Pérot resonator. The pump depletion effect acts as the additional constraint on the formation of effective Rayleigh mirrors, managing to a narrow-band radiation with a sub-kHz linewidth. Additionally, the random-lasing light is mixed with the pump light. The power spectrum of the optical heterodyne mixing product in the photodetector current is the convolution of the random laser spectrum with the pump laser spectrum. The random laser linewidth is small compared to the pump under test, so the convolution can trace out the test-laser

lineshape that is replicated at a low frequency, accessible to the electronics, set by the average optical frequency difference between the random laser and the pump laser. The sub-kHz spectral resolution of the linewidth measurement has eventually been realised. Meanwhile, an application in random bits generation at fast rates of up to 7.1 Mbit/s has also been achieved based on the stochastic power fluctuations of laser output.

We hope that this thesis will spark further interest in the reliable applications using the inherent features of random distributed fibre lasers. Further work could also look into exploiting the possibility of the application of the random Brillouin fibre laser in remote sensing and the application of different optical fibres to random laser system.

Chapter 7

Bibliography

[1] D. S. Wiersma, "Disordered photonics," *Nature Photon.* **7**, 188–196 (2010).

[2] P. W. Anderson, "The question of classical localization: A theory of white paint?," *Phil. Mag. B* **52**, 505–509 (1985).

[3] D. S. Wiersma, M. P. van Albada, A. Lagendijk, "Random laser?," *Nature* **373**, 203–204 (1995).

[4] H. Cao, "Lasing in random media," *Waves in random media* **13**, R1–R39 (2003).

[5] S. K. Turitsyn, S. A. Babin, A. E. El-Taher, P. Harper, D. V. Churkin, S. I. Kablukov, J. D. Ania-Castanon, V. Karalekas, E. V. Podivilov, "Random distributed feedback fibre laser," *Nature Photon.* **4**, 231–235 (2010).

[6] A. Burin, M. A. Ratner, H. Cao, and S. Chang, "Random laser in one dimension," *Phys. Rev. Lett.* **88**, 093904 (2002).

[7] C. J. S. de Matos, L. d. S. Menezes, A. M. Brito-Silva, M. A. M. Gámez, A. S. L. Gomes, C. B. de Araújo, "Random fibre laser," *Phys. Rev. Lett.* **99**, 153903 (2007).

[8] Z. Hu, *et al.* "Coherent random fibre laser based on nanoparticles scattering in the extremely weakly scattering regime," *Phys. Rev. Lett.* **109**, 253901 (2012).

[9] R. W. Boyd, K. Rzążewski, and P. Narum, "Noise initiation of stimulated Brillouin scattering," *Phys. Rev. A* **42**, 5514–5521 (1990).

[10] A. L. Gaeta, and R. W. Boyd. "Stochastic dynamics of stimulated Brillouin scattering in an optical fibre," *Phys. Rev. A* 44, 3205–3209 (1991).

[11] R. W. Boyd, Nonlinear Optics 3rd edn. New York: Academic Press, 2008.

[12] G. P Agrawal, Nonlinear Fibre Optics 5th edn. New York: Academic Press, 2013.

[13] K. Okamoto, Fundamentals of Optical Waveguides 2nd edn. New York: Academic Press, 2010.

[14] R. Hui, and M. O'Sullivan, Fibre Optic Measurement Techniques. New York: Academic Press, 2009.

[15] S. Sugavanam, N. Tarasov, X. Shu, D. V. Churkin, "Narrow-band generation in random distributed feedback fibre laser," *Opt. Express* **21**, 16466–16472 (2013).

[16] N. Lizaraga, N. P. Puente, E. I. Chaikina, T. A. Leskova, and E. R. Mendez, "Single-mode Er-doped fibre random laser with distributed Bragg grating

feedback," *Opt. Express* **17**, 395–404 (2009).

[17] M. Gagne and R. Kashyap, "Demonstration of a 3 mW threshold Er-doped random fibre laser based on a unique fibre Bragg grating," *Opt. Express* **17**, 19067–19074 (2009).

[18] Y. Li, *et al.* "Narrow linewidth low frequency noise Er-doped fibre ring laser based on femtosecond laser induced random feedback," ," *Appl. Phys. Lett.* **105**, 101105 (2014).

[19] A. A. Fotiadi, R. V. Kiyan, "Cooperative stimulated Brillouin and Rayleigh backscattering process in optical fibre," *Opt. Lett.* **23**, 1805–1807 (1998).

[20] M. Pang, S. Xie, X. Bao, D. Zhou, Y. Lu, and L.Chen, "Rayleigh scattering-assisted narrow linewidth Brillouin lasing in cascaded fibre," *Opt. Lett.* **37**, 3129–3131 (2012).

[21] B. Saxena, X. Bao, and L. Chen, "Suppression of thermal frequency noise in erbium-doped fibre random lasers," *Opt. Lett.* **39**, 1038–1041 (2014).

[22] J. Yao, "Microwave photonics," *J. Lightw. Technol.* **27**, 314–335 (2009).

[23] X. S. Yao, L. Maleki, "Optoelectronic Oscillator for Photonic Systems," *IEEE J. Quantum Electron.* **32**, 1141–1149 (1996).

[24] A. J. Seeds, K.J. Williams, "Microwave photonics," *J. Lightwave. Technol.* **24**, 4628–4641 (2006).

[25] C. Lim, A. Nirmalathas, M. Bakaul, K. L. Lee, D. Novak, R. Waterhouse, "Mitigation strategy for transmission impairments in millimeter-wave radio-over-fibre networks," *J. Opt. Netw.* **8**, 201–214 (2009).

[26] G. J. Simonis, D. G. Purchase, "Optical generation, distribution, and control of microwaves using laser heterodyne," *IEEE Trans. Microw. Theory. Tech.* **38**, 667–669 (1990).

[27] S. Latkowski, *et al*. "Analysis of a narrowband terahertz signal generated by a unitravelling carrier photodiode coupled with a dual-mode semiconductor Fabry-Pérot laser," *Appl. Phys. Lett.* **96**, 241106 (2010).

[28] G. Pillet, *et al*. "Dual-Frequency Laser at 1.5 μm for Optical Distribution and Generation of High-Purity Microwave Signals," *J. Lightwave. Technol.* **26**, 2764–2772 (2008).

[29] M. C. Gross, P. T. Callahan, T. R. Clark, D. Novak, R. B. Waterhouse, M. L. Dennis, "Tunable millimeter-wave frequency synthesis up to 100 GHz by dual-wavelength Brillouin fibre laser," *Opt. Express* **18**, 13321–13330 (2010).

[30] G. Ducournau, *et al*. "Highly coherent terahertz wave generation with a dual-frequency Brillouin fibre laser and a 1.55 μm photomixer," *Opt. Lett.* **36**, 2044–2046 (2011).

[31] J. Liu, *et al*. "Generation of step-tunable microwave signal using a multiwavelength Brillouin fibre laser," *IEEE Photon. Technol. Lett.* **25**, 220–223

(2013).

[32] J. Geng, S. Staines, S. Jiang, “Dual-frequency Brillouin fibre laser for optical generation of tunable low-noise radio frequency/microwave frequency,” *Opt. Lett.* **33**, 16–18 (2008).

[33] X. S. Yao, “High-quality microwave signal generation by use of Brillouin scattering in optical fibres,” *Opt. Lett.* **22**, 1329–1331 (1997).

[34] W. Lu, A. Johnstone, and R. G. Harrison, “Deterministic dynamics of stimulated scattering phenomena with external feedback,” *Phys. Rev. A* **46**, 4114–4122 (1992).

[35] A. A. Fotiadi, “Random lasers: An incoherent fibre laser,” *Nature Photon.* **4**, 204–205 (2010).

[36] A. Yariv, P. Yeh, *Photonics: Optical Electronics in Modern Communications 6th edn*. New York: Oxford University Press, 2007.

[37] P. B. Gallion, G. Debarge, “Quantum Phase Noise and Field Correlation in Single Frequency Semiconductor Laser Systems,” *IEEE J. Quantum Electron.* **20**, 343–349 (1984).

[38] D. Derickson, *Fibre Optic Test and Mearsurement*. Upper Saddle River: Prentice Hall, 1998.

[39] H. E. Rowe, *Signal and Noise in Communication Systems*. Toronto: Van Nostrand, 1965.

[40] M. Tonouchi, “Cutting-edge terahertz technology,” *Nature Photon.* **1**, 97–105 (2007).

[41] J. C. Juarez, E. W. Maier, N. C. Kyoo, H. F. Taylor, “Distributed fibre-optic intrusion sensor system,” *J. Lightwave Technol.* **23**, 2081–2087 (2005).

[42] A. Uchida, *et al*. “Fast physical random bit generation with chaotic semiconductor lasers,” *Nature Photon.* **2**, 728–732 (2008).

[43] A Tonello, *et al*. “Secret key exchange in ultralong lasers by radiofrequency spectrum coding,” *Light: Science & Applications* **4**, e276 (2015).

[44] E. Ip, A. P. Lau, D. J. Barros, and J. M. Kahn, “Coherent detection in optical fibre systems,” *Opt. Express* **16**, 753–791 (2008).

[45] J. Subías, C. Heras, J. Pelayo, and F. Villuendas, “All in fibre optical frequency metrology by selective Brillouin amplification of single peak in an optical comb,” *Opt. Express* **17**, 6753–6758 (2009).

[46] D. Guyomarc’h, G. Hagel, C. Zumsteg, and M. Knoop, “Some aspects of simulation and realization of an optical reference cavity,” *Phys. Rev. A* **80**, 063820 (2009).

[47] J. M. Campos, A. Destrez, J. Jacquet and Z. Toffano, “Ultra-fast optical spectrum analyzer for DWDM applications,” *IEEE Trans. Instrum. Meas.* **53**, 124–129 (2004).

[48] T. Takakura, K. Iga, T. Tako, “Linewidth measurement of a single longitudinal mode AlGaAs laser with Fabry-Perot Interferometer,” *Jpn. J. Appl. Phys.* **19**, L725–L727 (1980).

[49] H. Ludvigsen, M. Tossavainen, and M. Kaivola, “Laser linewidth measurements using self-homodyne detection with short delay,” *Opt. Commun.* **155**, 180–186 (1998).

[50] P. Horak, and W. H. Loh, “On the delayed self-heterodyne interferometric technique for determining the linewidth of fibre lasers,” *Opt. Express* **14**, 3923–3928 (2006).

[51] M. Han, A. Wang, “Analysis of a loss-compensated recirculating delayed self-heterodyne interferometer for laser linewidth measurement, ” *Appl. Phys. B* **81**, 53–58 (2005).

[52] X. Chen, M. Han, Y. Zhu, B. Dong and A. Wang, “Implementation of a loss-compensated recirculating delayed self-heterodyne interferometer for ultranarrow laser linewidth measurement, ” *Appl. Opt.* **45**, 7712–7717 (2006).

[53] J. M. S. Domingo, J. Pelayo, F. Villuendas, C. D. Heras, and E. Pellejer, “Very High Resolution Optical Spectrometry by Stimulated Brillouin Scattering,” *IEEE Photon. Technol. Lett.* **17**, 855–857 (2005).

[54] P. Sevillano, J. Subías, C. Heras, J. Pelayo and F. Villuendas, “Brillouin induced self-heterodyne technique for narrow line width measurement,” *Opt. Express* **18**, 15201–15206 (2010).

[55] F. Mihélic, D. Bacquet, J. Zemmouri, and P. Szriftgiser, “Ultrahigh resolution spectral analysis based on a Brillouin fibre laser,” *Opt. Lett.* **35**, 432–434 (2010).

[56] X. Bao, and L. Chen, “Recent progress in Brillouin scattering based fibre sensors,” *Sensors* **11**, 4152–4187 (2011).

[57] A. J. Menezes, P. C. van Oorschot, and S. A. Vanstone, *Handbook of Applied Cryptography*. Boca Raton: CRC press, 1996.

[58] N. Metropolis and S. Ulam, “The monte carlo method,” *J. Am. Stat. Assoc.* **44**, 335–341 (1949).

[59] S. Asmussen and P. W. Glynn, *Stochastic Simulation:Algorithms and Analysis*. New York: Springer-Verlag, 2007.

[60] T. E. Murphy, and R. Roy, “Chaotic lasers: The world's fastest dice,” *Nature Photon.* **2**, 714–715 (2008).

[61] W. T. Holman, J. A. Connelly, and A. B. Dowlatabadi, “An integrated analog/digital random noise source,” *IEEE Trans. Circuits and Systems I* **44**, 521–528 (1997).

[62] J. F. Dynes, Z. L. Yuan, A. W. Sharpe, and A. J. Shields, "A high speed, post-processing free, quantum random number generator," *Appl. Phys. Lett.* **93**, 031109 (2008).

[63] Uchida, Atsushi, *et al*. "Fast physical random bit generation with chaotic semiconductor lasers, " *Nature Photon.* **2**, 728–732 (2008).

[64] C. R. S. Williams, J. C. Salevan, X. Li, R. Roy, and T. E. Murphy, "Fast physical random number generator using amplified spontaneous emission," *Opt. Express* **18**, 23584–23597 (2010).

[65] H. Guo, W. Tang, Y. Liu, and W. Wei, "Truly random number generation based on measurement of phase noise of a laser," *Phys. Rev. E* **81**, 051137 (2010).

[66] D. S. Wiersma, "The physics and applications of random lasers," *Nature Phys.* **4**, 359–367 (2008).